A consistent third-order propagator method for electronic excitation

A. B. Trofimov,[a] G. Stelter, and J. Schirmer
Physikalisch-Chemisches Institut, University of Heidelberg, D-69120 Heidelberg, Germany

(Received 3 June 1999; accepted 9 September 1999)

A propagator method referred to as third-order algebraic–diagrammatic construction [ADC(3)] for the direct computation of electronic excitation energies and transition moments is presented. This approach is based on a specific reformulation of the diagrammatic perturbation expansion for the polarization propagator, and extends the existing second-order [ADC(2)] scheme to the next level of perturbation theory. The computational scheme combines diagonalization of a Hermitian secular matrix and perturbation theory for the matrix elements. The characteristic properties of the method are *compact* configuration spaces, *regular* perturbation expansions, and *size-consistent* results. The configuration space is spanned by singly and doubly excited states, while the perturbation expansions in the secular matrix extend through third order in the p-h block, second order in the p-h/$2p$-$2h$ coupling block, and first order in the $2p$-$2h$ block. While the simpler ADC(2) method, representing a counterpart to the MP2 (second-order Møller–Plesset) ground-state method, recommends itself for application to larger molecules, the ADC(3) scheme is aimed at a more accurate description of molecular excitation spectra. The relationship of the ADC(3) scheme with coupled cluster methods is discussed, focusing here in particular on the treatment of transition moments. © *1999 American Institute of Physics.* [S0021-9606(99)30345-7]

I. INTRODUCTION

As is well known, a central entity in the derivation of many-body methods for the treatment of electronic excitations in atoms and molecules is the polarization propagator.[1–3] Among the various computational schemes based on or related to the polarization propagator one may distinguish between algebraic methods and diagrammatic methods. Practical computational schemes of the former kind have been developed in the framework of the equation-of-motion method (EOM),[4–7] and the essentially equivalent superoperator formalism.[8–10] Following the diagrammatic approach, based on the diagrammatic perturbation expansion of the polarization propagator, a general procedure referred to as algebraic–diagrammatic construction (ADC)[11] has been used to derive approximation schemes beyond the level of the famous, though unsatisfactory, random-phase approximation (RPA). These many-body methods have two characteristic features. Firstly, the excitation energies and transition moments (spectral intensities) are determined directly, that is, without the need of performing separate calculations for the initial and final states, as is the case in the conventional wave function approach. Secondly, the methods are potentially size-consistent (here, more specifically, size-intensive) which is crucial in the application to larger systems. Whether a method is size-intensive can be seen in the application to a system consisting of two separate (noninteracting) fragments. Here the resulting excitation energies and transition moments for a local excitation should not depend on whether the method is applied to the whole system or to the concerned fragment.

In practice, the resulting computational schemes combine in one form or another the solution of secular equations (eigenvalue problem) with perturbation theory in form of finite expansions for the secular matrix elements or related quantities. A (not necessarily sufficient) measure of the general quality of the approximation scheme is the perturbation theoretical consistency of the results for, say, the class of single or particle-hole (p-h) excitations. For example, the RPA is only a first-order method, as the error introduced here both for the (p-h) excitation energies and transition moments is of second order. A substantial improvement of the results was achieved by second-order methods, such as the SOPPA (second-order polarization propagator approximation) method[9,12,13] derived within the EOM/superoperator approach, or the second-order ADC(2) scheme.[11,14] A third-order extension of the algebraic EOM/superoperator formulation has been presented in Ref. 15, but, to the best of our knowledge, this scheme has never been implemented in a computer code nor used in actual applications. While the available second-order schemes are quite practical and efficient (the computational effort may be compared to that of the familiar SDCI (configuration interaction including all single and double excitations on the Hartree–Fock (HF) reference state), the accuracy, say, for the p-h excitation energies is comparable to that of the widely applied MP2 (Møller–Plesset second-order perturbation theory) method for the ground-state energy. Typically one has to expect an error of ± 0.5 eV for the p-h excitation energies which is clearly inferior to the accuracy standard of the successful CASPT2 [complete active space multireference SCF (self-consistent field) plus second-order perturbation theory] method.[16,17] The relative modest performance of second-order methods is a well-known fact in the related field of electronic ionization, where for a long time third-order

[a]Permanent address: Laboratory of Quantum Chemistry, Computer Center, Irkutsk State University, 664003 Irkutsk, Russian Federation.

propagator and related methods have been used with considerable success.[7,18–21] The claimed accuracy standard here is ± 0.2 eV for the ionic main states (single hole states). In view of this situation the development of a consistent third-order method for electronic excitations would be highly desirable, and one may wonder why such a scheme has not emerged as yet.

In this article we will extend the ADC procedure beyond second-order and derive complete third-order [ADC(3)] equations for the polarization propagator. The derivation reveals a substantial complexity inherent to this level of approximation which apparently has discouraged previous attempts to develop third-order schemes for electronic excitation. Compared to the electron propagator (one-particle Green's function) in the ionization problem, the complexity encountered here is greater by one order of magnitude. This holds in particular for the calculation of the third-order transition moments. For the excitation energies, however, the situation is more favorable. As will be seen, the ADC(3) expressions for the secular matrix are not at odds with the end of devising a both efficient and accurate computational scheme. Like at the second-order level, the explicit configuration space of the ADC(3) secular matrix is spanned by the manifold of singly and doubly excited states. An apparent bottleneck is the plethora of 29 distinct third-order contributions to the p-h block of the secular matrix leading to a N^8 scaling in the computation of this block.

The ADC reformulation of the polarization propagator can be introduced in an alternative way as a so-called intermediate state (ISR) representation[22] of the (shifted) Hamiltonian $\hat{H}-E_0$, where E_0 is the exact ground-state energy. This point of view puts the ADC approach directly into the context of methods extending the successful coupled cluster (CC) method to the treatment of electronic transitions. Methods of this type are the multireference coupled cluster (MRCC) schemes,[23,24] the SAC-CI (symmetry adapted cluster) method,[25–27] the coupled cluster linear response (CCLR) theory,[28–32] and the equation-of-motion coupled cluster (EOM-CC) method.[33–35] For a general discussion of various aspects of these ISR methods, the reader is referred to Ref. 22. In contrast to the EOM/superoperator and ADC schemes, the CC methods are basically nonperturbative (the secular matrix elements here are constructed from terms generated by a CC ground-state calculation). However, it should be noted, that most CC schemes reported so far are only consistent through second order for the energies and transition moments. A consistent third-order method referred to as CC3 model has been presented by Christiansen *et al.*[36] A comparison of the ADC approach and CC methods is given in Sec. V B.

II. ALGEBRAIC–DIAGRAMMATIC CONSTRUCTION (ADC) FOR THE POLARIZATION PROPAGATOR

In the following we will briefly review the polarization propagator and the general aspects of the ADC approach. For the original derivation and further details the reader is referred to Ref. 11.

A. Review of the polarization propagator

The polarization propagator is defined as a matrix $\mathbf{\Pi}(\omega)$ of energy (or time-) dependent functions[1]

$$\Pi_{rs,r's'}(\omega)=\Pi^{+}_{rs,r's'}(\omega)+\Pi^{-}_{rs,r's'}(\omega) \tag{1a}$$

$$\Pi^{+}_{rs,r's'}(\omega)=\langle\Psi_0|c_s^{\dagger}c_r(\omega-\hat{H}+E_0+i\eta)^{-1}\hat{Q}_0c_{r'}^{\dagger}c_{s'}|\Psi_0\rangle, \tag{1b}$$

$$\Pi^{-}_{rs,r's'}(\omega)=\Pi^{+}_{s'r',sr}(-\omega). \tag{1c}$$

Here we consider an N-electron system with a (nondegenerate) ground-state $|\Psi_0\rangle$ and energy E_0. Moreover, we assume a single-particle representation based on the ground-state Hartree–Fock (HF) orbitals $|\varphi_p\rangle$. The associated creation (annihilation) operators of second quantization are denoted by $c_p^{\dagger}(c_p)$. $\hat{H}$ is the Hamiltonian of the system, and

$$\hat{Q}_0=\hat{1}-|\Psi_0\rangle\langle\Psi_0|, \tag{2}$$

denotes the projection operator onto the orthogonal complement of the exact ground-state $|\Psi_0\rangle$. The positive infinitesimal η, guaranteeing the convergence of the Fourier transformations between time and energy representations, will be dropped in the following whenever unessential. According Eq. (1), the polarization propagator consists of two parts, $\mathbf{\Pi}^{+}(\omega)$ and $\mathbf{\Pi}^{-}(\omega)$, which are related by Eq. (1c). Therefore, it suffices to confine oneself to the part $\mathbf{\Pi}^{+}(\omega)$. The physical content of $\mathbf{\Pi}^{+}(\omega)$ is explicit in the so called spectral representation[1] reading in a compact matrix notation

$$\mathbf{\Pi}^{+}(\omega)=\boldsymbol{x}^{\dagger}(\omega-\mathbf{\Omega})^{-1}\boldsymbol{x}. \tag{3}$$

Here $\mathbf{\Omega}$ is the diagonal matrix of (vertical) excitation energies

$$\omega_m=E_m-E_0, \tag{4}$$

and $\boldsymbol{x}$ is the matrix of transition amplitudes

$$x_{m,rs}=\langle\Psi_m|c_r^{\dagger}c_s|\Psi_0\rangle. \tag{5}$$

The latter amplitudes enter the calculation of spectral intensities as follows. Let

$$\hat{D}=\sum_{r,s} d_{rs}c_r^{\dagger}c_s, \tag{6}$$

denote a single-particle transition operator (e.g., the z component of the dipole operator), where d_{rs} are the associated one-particle integrals (e.g., $d_{rs}=\langle\varphi_r|\hat{z}|\varphi_s\rangle$). Then the transition moment for the $0\rightarrow m$ transition can be written in the form

$$T_m=\langle\Psi_m|\hat{D}|\Psi_0\rangle=\sum_{r,s} x_{m,rs}d_{rs}. \tag{7}$$

The well-known formalism of diagrammatic perturbation theory (see, for example, Fetter and Walecka[1]) allows one to construct the perturbation expansion of the polarization propagator in terms of the famous Feynman diagrams. Figures 1 and 2 show the Feynman diagrams (in Abrikosov or Hugenholz form) through second and in third order, respectively. According to the diagram rules, an nth order

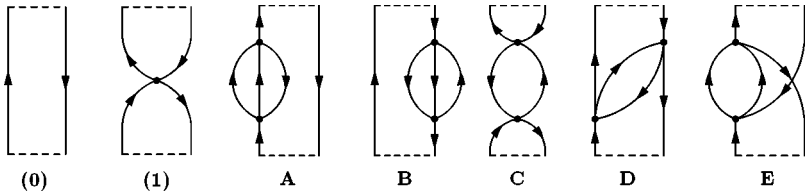

FIG. 1. Feynman diagrams for the polarization propagator through second order.

Feynman diagram introduces an n-fold energy (or time) integration over the arguments of the n inner vertices. Explicit analytical expressions for the result of the internal integrations can be obtained from the so-called time-ordered or Goldstone diagrams.[1] In nth order each Feynman diagram gives rise to $(n+2)!$ Goldstone diagrams. (For the diagram rules and an example see Appendix A.)

The time ordered diagrams decompose into two distinct classes, I and II, corresponding to the two possible time orderings of the external vertices t and t'. Class I ($t>t'$) and class II ($t<t'$) contribute exclusively to $\mathbf{\Pi}^+$ and $\mathbf{\Pi}^-$, respectively. This establishes a direct diagrammatic perturbation expansion for the part $\mathbf{\Pi}^+$ to be considered below. For the second-order diagram C the 12 Goldstone diagrams contributing to $\mathbf{\Pi}^+$ are shown in Fig. 3. In third order there are already 60 Goldstone diagrams for $\mathbf{\Pi}^+$ per Feynman diagram [see Fig. 4 displaying the diagrams associated with the Feynman diagram (7)].

B. General ADC equations

In the ADC formulation the polarization propagator part $\mathbf{\Pi}^+(\omega)$ is written in the general algebraic form

$$\mathbf{\Pi}^+(\omega)=\boldsymbol{f}^\dagger(\omega-\boldsymbol{K}-\boldsymbol{C})^{-1}\boldsymbol{f}. \tag{8}$$

This nondiagonal representation may be established in a similar way as the (diagonal) spectral representation [Eq. (3)] by inserting a complete set of so-called intermediate states $|\tilde{\Psi}_J\rangle$ on the right-hand-side of Eq. (1b) instead of the exact excited states (see Sec. V B). These states are labeled like the usual excitation manifold of p-h (particle-hole), $2p$-$2h$, $3p$-$3h$ . . . -excitations, that is

$$\{J\}\equiv\{aj,\ abij,\ \ldots;a<b,i<j;\ \ldots\}.$$

Here and in the following we adopt the usual convention to designate occupied orbitals by $i,j,k,l,\ldots$, unoccupied (virtual) orbitals by $a,b,c,\ldots$, and unspecified orbitals by $p,q,r,\ldots$. The secular matrix $\boldsymbol{K}+\boldsymbol{C}$ introduced in Eq. (8) is defined according to

$$(\boldsymbol{K}+\boldsymbol{C})_{IJ}=\langle\tilde{\Psi}_I|\hat{H}-E_0|\tilde{\Psi}_J\rangle, \tag{9}$$

as the intermediate state representation of the (shifted) Hamiltonian $\hat{H}-E_0$, while the matrix $\boldsymbol{f}$ of ''effective'' transition amplitudes is given by

$$f_{I,rs}=\langle\tilde{\Psi}_I|c_r^\dagger c_s|\Psi_0\rangle. \tag{10}$$

The ADC procedure aims directly at determining the secular matrix $\boldsymbol{K}+\boldsymbol{C}$ and the effective transition amplitudes $\boldsymbol{f}$, assuming that these quantities can be expanded in perturbation series

$$\begin{aligned}\boldsymbol{C}&=\boldsymbol{C}^{(1)}+\boldsymbol{C}^{(2)}+\boldsymbol{C}^{(3)}\cdots,\\ \boldsymbol{f}&=\boldsymbol{f}^{(0)}+\boldsymbol{f}^{(1)}+\boldsymbol{f}^{(2)}\cdots,\end{aligned} \tag{11}$$

with respect to the usual Møller–Plesset partitioning $\hat{H}=\hat{H}_0+\hat{H}_I$ of the Hamiltonian. The zeroth-order (or HF) part of the secular matrix is given by the diagonal matrix $\boldsymbol{K}$ of HF excitation energies, that is

$$\begin{aligned}K_{ak,ak}&=\epsilon_a-\epsilon_k,\\ K_{abkl,abkl}&=\epsilon_a+\epsilon_b-\epsilon_k-\epsilon_l,\end{aligned} \tag{12}$$

and so forth, where the ϵ_p denote HF orbital energies. Inserting the expansions of Eq. (11) in the ADC form [Eq. (8)] generates a perturbation expansion for the ADC form of $\mathbf{\Pi}^+(\omega)$, which now can be compared with the original dia-

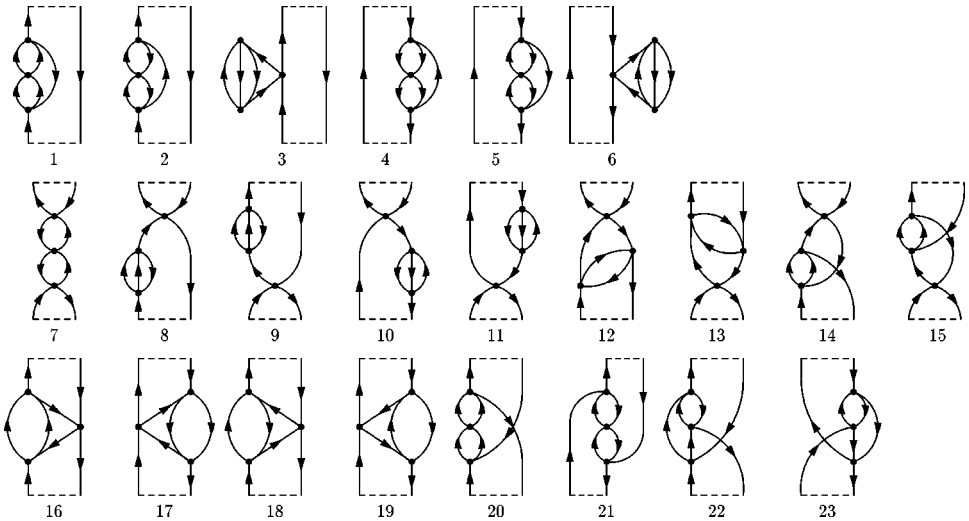

FIG. 2. Third-order Feynman diagrams for the polarization propagator.

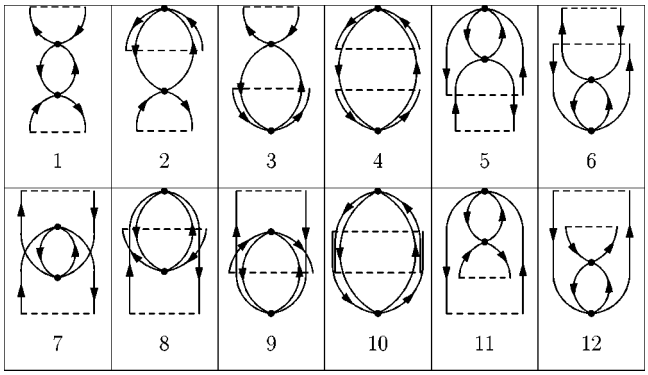

FIG. 3. Goldstone diagrams associated with the second-order Feynman diagram (C); only diagrams contributing to $\mathbf{\Pi}^+$ are shown.

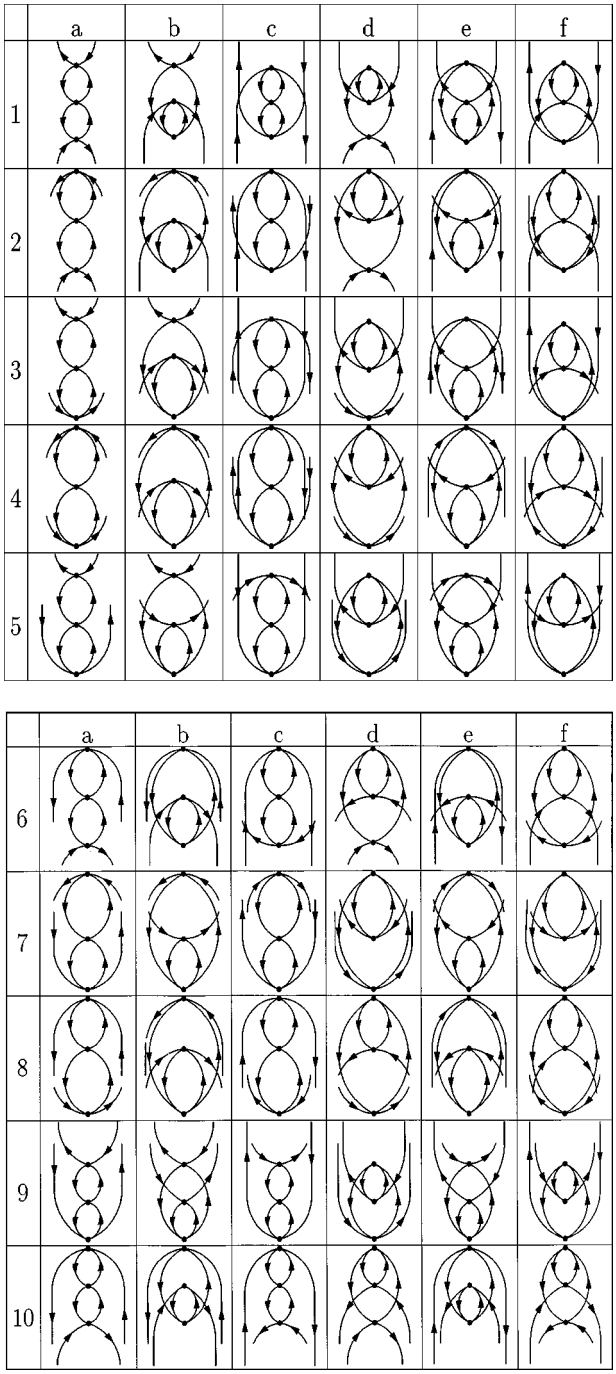

FIG. 4. Goldstone diagrams associated with the third-order Feynman diagram (7); only diagrams contributing to $\mathbf{\Pi}^+$ are shown.

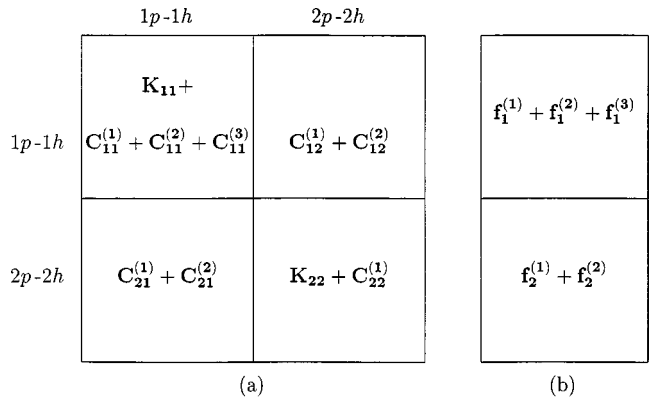

FIG. 5. Block structure of the secular matrix $\boldsymbol{K}+\boldsymbol{C}$ (a) and of the effective transition amplitude matrix $\boldsymbol{f}$ (b) of the third-order ADC scheme.

grammatic series for $\mathbf{\Pi}^+(\omega)$. This allows one to determine the contributions to $\boldsymbol{C}$ and $\boldsymbol{f}$ successively through higher order.

The structure of the secular matrix $\boldsymbol{K}+\boldsymbol{C}$ and of the $\boldsymbol{f}$ matrix in the third-order ADC approximation scheme (resulting from the comparison through third order) is depicted in Fig. 5. The explicit configuration space here comprises the p-h excitations (class $\mu=1$) and the $2p$-$2h$ excitations (class $\mu=2$). The perturbation expansions for the different blocks $\boldsymbol{C}_{\mu,\mu'}$, $\mu,\mu'=1,2$ of $\boldsymbol{C}$ are as follows:

$$\begin{aligned}
\boldsymbol{C}_{11}&=\boldsymbol{C}_{11}^{(1)}+\boldsymbol{C}_{11}^{(2)}+\boldsymbol{C}_{11}^{(3)},\\
\boldsymbol{C}_{12}&=\boldsymbol{C}_{12}^{(1)}+\boldsymbol{C}_{12}^{(2)},\\
\boldsymbol{C}_{22}&=\boldsymbol{C}_{22}^{(1)}.
\end{aligned} \tag{13}$$

In a similar way one may distinguish the blocks $\boldsymbol{f}_\mu$, $\mu=1,2$, of effective transition amplitudes. Here the perturbation expansions of the ADC(3) scheme read

$$\begin{aligned}
\boldsymbol{f}_1&=\boldsymbol{f}_1^{(0)}+\boldsymbol{f}_1^{(1)}+\boldsymbol{f}_1^{(2)}+\boldsymbol{f}_1^{(3)},\\
\boldsymbol{f}_2&=\boldsymbol{f}_2^{(1)}+\boldsymbol{f}_2^{(2)}.
\end{aligned} \tag{14}$$

For further reference we also introduce the notation $\boldsymbol{f}_{\mu\mathbf{1}}$ and $\boldsymbol{f}_{\mu\bar{\mathbf{1}}}$ for the subblocks of $\boldsymbol{f}_\mu$ where the second index pair rs is a ph pair (1) or any of the possibilities hp,hh,pp $(\bar{1})$, respectively. The respective terms of highest order in Eqs. (13) and (14) are to be determined at the third-order level of $\mathbf{\Pi}^+(\omega)$ (see Sec. III); the lower order terms follow from the ADC procedure through second order.[11]

For a given secular matrix $\boldsymbol{K}+\boldsymbol{C}$ the excitation energies ω_m are obtained from the solution of the (Hermitian) eigenvalue problem

$$(\boldsymbol{K}+\boldsymbol{C})\boldsymbol{Y}=\boldsymbol{Y}\mathbf{\Omega},\quad \boldsymbol{Y}^\dagger\boldsymbol{Y}=\mathbf{1}. \tag{15}$$

Here $\mathbf{\Omega}$ is the diagonal matrix of eigenvalues ω_m, and $\boldsymbol{Y}$ denotes the matrix of eigenvectors. The transition moments [Eq. (7)] are given by the scalar products

$$T_m=\underline{Y}^{(m)^\dagger}\underline{F}, \tag{16}$$

of the mth eigenvector and the vector of effective transition moments

TABLE I. Second-order contributions in the ADC representation [Eq. (8)] of $\mathbf{\Pi}^+(\omega)$.

(A)	$\boldsymbol{f}_1^{(2)^\dagger}\boldsymbol{\omega}_1^{-1}\boldsymbol{f}_1^{(0)}+\text{h.c.}$
(B)	$\boldsymbol{f}_1^{(1)^\dagger}\boldsymbol{\omega}_1^{-1}\boldsymbol{f}_1^{(1)}$
(C)	$\boldsymbol{f}_1^{(1)^\dagger}\boldsymbol{\omega}_1^{-1}\boldsymbol{C}_{11}^{(1)}\boldsymbol{\omega}_1^{-1}\boldsymbol{f}_1^{(0)}+\text{h.c.}$
(D)	$\boldsymbol{f}_1^{(0)^\dagger}\boldsymbol{\omega}_1^{-1}\boldsymbol{C}_{11}^{(1)}\boldsymbol{\omega}_1^{-1}\boldsymbol{C}_{11}^{(1)}\boldsymbol{\omega}_1^{-1}\boldsymbol{f}_1^{(0)}$
(E)	$\boldsymbol{f}_1^{(0)^\dagger}\boldsymbol{\omega}_1^{-1}\boldsymbol{C}_{11}^{(2)}\boldsymbol{\omega}_1^{-1}\boldsymbol{f}_1^{(0)}$
(F)	$\boldsymbol{f}_2^{(1)^\dagger}\boldsymbol{\omega}_2^{-1}\boldsymbol{f}_2^{(1)}$
(G)	$\boldsymbol{f}_2^{(1)^\dagger}\boldsymbol{\omega}_2^{-1}\boldsymbol{C}_{21}^{(1)}\boldsymbol{\omega}_1^{-1}\boldsymbol{f}_1^{(0)}+\text{h.c.}$
(H)	$\boldsymbol{f}_1^{(1)^\dagger}\boldsymbol{\omega}_1^{-1}\boldsymbol{C}_{12}^{(1)}\boldsymbol{\omega}_2^{-1}\boldsymbol{C}_{21}^{(1)}\boldsymbol{\omega}_1^{-1}\boldsymbol{f}_1^{(0)}$

$$F_J=\sum_{r,s} f_{J,rs}d_{rs}, \tag{17}$$

where d_{rs} are the one-particle integrals of the considered transition operator.

III. EXPLICIT ADC EXPRESSIONS THROUGH THIRD ORDER

In Ref. 11 the derivation of the explicit ADC equations for $\mathbf{\Pi}^+$ through second order has been described. In the following we will extend this procedure to third order (Secs. III B and III C). As a preparation to this steps it should be useful to recall briefly the much simpler first- and second-order cases.

A. First- and second-order ADC schemes

In zeroth and first order the ADC form [Eq. (8)] reads

$$\begin{aligned}\mathbf{\Pi}^+(\omega)=&\boldsymbol{f}_1^{(0)^\dagger}\boldsymbol{\omega}_1^{-1}\boldsymbol{f}_1^{(0)}+\boldsymbol{f}_1^{(0)^\dagger}\boldsymbol{\omega}_1^{-1}\boldsymbol{C}_{11}^{(1)}\boldsymbol{\omega}_1^{-1}\boldsymbol{f}_1^{(0)}\\&+\boldsymbol{f}_1^{(0)^\dagger}\boldsymbol{\omega}_1^{-1}\boldsymbol{f}_1^{(1)}+\boldsymbol{f}_1^{(1)^\dagger}\boldsymbol{\omega}_1^{-1}\boldsymbol{f}_1^{(0)},\end{aligned} \tag{18}$$

involving only p-h blocks ($\mu=1$) of $\boldsymbol{f}$ and $\boldsymbol{K}+\boldsymbol{C}$. Here and in the following the short hand-notation

$$\omega_\mu=(\omega-\boldsymbol{K})_\mu \tag{19}$$

is used. The zeroth- and first-order diagrams (Fig. 1) for $\mathbf{\Pi}^+$ fit directly to the ADC form [Eq. (18)], so that the quantities $\boldsymbol{C}_{11}^{(1)}$, $\boldsymbol{f}_1^{(0)}$, and $\boldsymbol{f}_1^{(1)}$ can simply be read off the analytical expressions yielding

$$C^{(1)}_{ak,a'k'}=-V_{ak'[a'k]},\quad f^{(0)}_{ak,rs}=\delta_{ar}\delta_{ks}, \tag{20}$$

$$\begin{aligned}f^{(1)}_{ak,k'a'}&=\frac{V_{aa'[k'k]}}{\epsilon_a+\epsilon_{a'}-\epsilon_k-\epsilon_{k'}},\\ f^{(1)}_{ak,a'k'}&=f^{(1)}_{ak,a'b'}=f^{(1)}_{ak,k'l'}=0,\end{aligned} \tag{21}$$

where $V_{pq[rs]}=V_{pqrs}-V_{pqsr}$ denote the antisymmetrized Coulomb integrals (in ''1212'' notation).

In second order there are eight contributions (A)–(H) for the ADC form [Eq. (8)] as listed in Table I. Here the terms (F)–(H) show that the next higher configuration class, that is, the $2p$-$2h$ excitations ($\mu=2$), comes explicitly into play. The ADC quantities to be determined at this level are $\boldsymbol{C}_{11}^{(2)}$, $\boldsymbol{C}_{12}^{(1)}$, $\boldsymbol{f}_1^{(2)}$, and $\boldsymbol{f}_2^{(1)}$. The terms of Table I have to be compared to the second-order Feynman diagrams in Fig. 1. Each of the five second-order Feynman diagrams (A)–(E) gives rise to 12 Goldstone diagrams contributing to $\mathbf{\Pi}^+(\omega)$, so that altogether a manifold of 60 diagrams has to be considered. As an example, Fig. 3 shows the Goldstone diagrams for the RPA diagram (C), labeled from (1)–(12). For most of the diagrams the assignment to the ADC terms is straightforward, since their analytical expressions fit directly to corresponding terms in Table I. Only 12 diagrams, more specifically, the Goldstone diagrams (time orderings) (7)–(10) of Feynman diagrams (A)–(C) require a simple algebraic transformation before they assume a compatible form. Let us consider the diagrams in Fig. 3. Obviously, diagram (1) corresponds to term (D), and merely repeats quantities already determined at the first-order level. In the following such diagrams are termed as repetitive diagrams or as diagrams containing repetitive terms. The latter also holds for diagram (2) and its Hermitian conjugate diagram (3) corresponding to term (C), as well as for diagram (4) being of the form of term (B). The diagrams (5), (11), and their Hermitian conjugated counterparts (6), (12) are of the form (A), thus specifying a contribution to $\boldsymbol{f}_1^{(2)}$.

The remaining four diagrams (7)–(10) do not fit individually to the ADC terms. Obviously, the corresponding analytic expressions $X(m)$, $m=7-10$ differ only in the denominator products $P(m)$, that is

$$X(m)=\sum_{i,c} V_{ac[ik]}V_{ik'[a'c]}P(m),$$

where

$$\begin{aligned}P(7)&=(\omega+\epsilon_k-\epsilon_a)^{-1}(\omega+\epsilon_{k'}-\epsilon_{a'})^{-1}\omega_6^{-1},\\ P(8)&=(\omega+\epsilon_{k'}-\epsilon_{a'})^{-1}\omega_6^{-1}\epsilon_1^{-1},\\ P(9)&=(\omega+\epsilon_k-\epsilon_a)^{-1}\omega_6^{-1}\epsilon_2^{-1},\\ P(10)&=\omega_6^{-1}\epsilon_1^{-1}\epsilon_2^{-1}.\end{aligned}$$

Here we use the abbreviations $\omega_6=(\omega+\epsilon_k+\epsilon_{k'}+\epsilon_i-\epsilon_a-\epsilon_{a'}-\epsilon_c)$, $\epsilon_1=(\epsilon_{k'}+\epsilon_i-\epsilon_{a'}-\epsilon_c)$, and $\epsilon_2=(\epsilon_k+\epsilon_i-\epsilon_a-\epsilon_c)$. All four denominator products share the factor ω_6^{-1} arising from the ''cut'' of three particle and three hole lines in the diagrams. Clearly the presence of this six-line denominator would not be compatible with the ADC scheme where explicit $3p$-$3h$ denominators occur for the first time at fourth order. Indeed, the ω_6^{-1} factor cancels when the four products $P(m)$ are added up, and the simple result is

$$\begin{aligned}\sum_{m=7}^{10}P(m)=&(\omega+\epsilon_k-\epsilon_a)^{-1}(\omega+\epsilon_{k'}-\epsilon_{a'})^{-1}\frac{\epsilon_1+\epsilon_2}{2\epsilon_1\epsilon_2}\\&+(\omega+\epsilon_k-\epsilon_a)^{-1}\frac{1}{2\epsilon_1\epsilon_2}\\&+(\omega+\epsilon_{k'}-\epsilon_{a'})^{-1}\frac{1}{2\epsilon_1\epsilon_2}.\end{aligned} \tag{22}$$

This shows, that the joint contribution of the diagrams (7)–(10) splits into a part being of the form (E) and two further parts being of the form (A).

The resulting contributions to $\boldsymbol{C}_{11}^{(2)}$ and $\boldsymbol{f}_{1}^{(2)}$ read

$$\tilde{C}_{ak,a'k'}^{(2)}=\sum_{i,c}\ V_{ac[ik]}V_{ik'[a'c]}\frac{\epsilon_1+\epsilon_2}{2\epsilon_1\epsilon_2}, \tag{23}$$

$$\tilde{f}_{ak,a'k'}^{(2)}=\frac{1}{2}\sum_{i,c}\ V_{ac[ik]}V_{ik'[a'c]}\frac{1}{\epsilon_1\epsilon_2}, \tag{24}$$

respectively. In a similar way one may analyze the Feynman diagrams (A) and (B).

A remark applies to the signs of the $\boldsymbol{C}_{12}^{(1)}$ and $\boldsymbol{f}_{2}^{(1)}$ contributions. Obviously, the terms (H) and (F) do not fix the overall sign of $\boldsymbol{C}_{12}^{(2)}$ and $\boldsymbol{f}_{2}^{(1)}$, respectively. This is to be expected as the phases of the $2p$-$2h$ states coming here into play need not be determined. However, the relative signs are not arbitrary, but have to be determined by inspecting (G).

B. Third-order ADC: General remarks

The derivation of the first- and second-order ADC schemes, as sketched in the preceding subsection, could be achieved without undue effort. At the third-order level, however, the complexity grows by an order of magnitude, which calls for reasonable handling strategies. As shown in Table II, the third-order ADC expansion can be broken into 20 individual terms labeled (A)–(T). Subscripts 1 and 2 will be used to distinguish between the term written out in Table II and its Hermitian counterpart (h.c.). The first nine terms (A)–(I) in Table II are pure p-h parts, the following terms (J)–(R) introduce mixing of the p-h and $2p$-$2h$-configurations, while the two remaining terms (S) and (T) are pure $2p$-$2h$-contributions. The new quantities to be determined at third order are $\boldsymbol{C}_{11}^{(3)}$, $\boldsymbol{C}_{12}^{(2)}$, $\boldsymbol{C}_{22}^{(1)}$, $\boldsymbol{f}_{1}^{(3)}$, and $\boldsymbol{f}_{2}^{(2)}$. These new quantities arise only in 9 terms of Table II, namely in (A), (G), (J)–(L), (P), (R)–(T). This means that the other 11 terms are mere repetitions of the quantities already determined at the first- and second-order level. Most of the latter terms can be readily assigned to individual third-order Goldstone diagrams.

The algebraic terms of Table II are opposed by an awesome number of third-order diagrams. As shown in Fig. 2 there are 23 Feynman diagrams, each contributing 60 Goldstone diagrams to $\boldsymbol{\Pi}^{+}$, which results in a total of 1380 Goldstone diagrams. As an example, Fig. 4 shows the 60 Goldstone diagrams associated with the third-order (RPA) diagram (7). For a unique designation of the diagrams we use the convention, $i.jx$, where $i=1,\ldots,23$ labels the Feynman diagrams as in Fig. 2, while the extension jx after the dot specifies the Goldstone diagrams as in Fig. 4. The first entry $j=1,\ldots,10$ distinguishes the positions of the two outer vertices according to the ten choices (1,5), (2,5), (1,4), (2,4), (1,3), (3,5), (2,3), (3,4), (1,2), and (4,5); for a given position of the two outer vertices the second entry $x=a,\ldots,f$ specifies the six permutations of the three inner vertices (123), (132), (321), (213), (312), and (231), where (123) is the order in the original Feynman diagram. Here the vertex numbering runs from the top to the bottom of the diagram.

TABLE II. Third-order contributions in the ADC representation [Eq. (8)] of $\boldsymbol{\Pi}^{+}(\omega)$.

(A)	$\boldsymbol{f}_1^{(3)^\dagger}\boldsymbol{\omega}_1^{-1}\boldsymbol{f}_1^{(0)}+\text{h.c.}$
(B)	$\boldsymbol{f}_1^{(2)^\dagger}\boldsymbol{\omega}_1^{-1}\boldsymbol{f}_1^{(1)}+\text{h.c.}$
(C)	$\boldsymbol{f}_1^{(2)^\dagger}\boldsymbol{\omega}_1^{-1}\boldsymbol{C}_{11}^{(1)}\boldsymbol{\omega}_1^{-1}\boldsymbol{f}_1^{(0)}+\text{h.c.}$
(D)	$\boldsymbol{f}_1^{(1)^\dagger}\boldsymbol{\omega}_1^{-1}\boldsymbol{C}_{11}^{(2)}\boldsymbol{\omega}_1^{-1}\boldsymbol{f}_1^{(0)}+\text{h.c.}$
(E)	$\boldsymbol{f}_1^{(1)^\dagger}\boldsymbol{\omega}_1^{-1}\boldsymbol{C}_{11}^{(1)}\boldsymbol{\omega}_1^{-1}\boldsymbol{f}_1^{(1)}$
(F)	$\boldsymbol{f}_1^{(1)^\dagger}\boldsymbol{\omega}_1^{-1}\boldsymbol{C}_{11}^{(1)}\boldsymbol{\omega}_1^{-1}\boldsymbol{C}_{11}^{(1)}\boldsymbol{\omega}_1^{-1}\boldsymbol{f}_1^{(0)}+\text{h.c.}$
(G)	$\boldsymbol{f}_1^{(0)^\dagger}\boldsymbol{\omega}_1^{-1}\boldsymbol{C}_{11}^{(3)}\boldsymbol{\omega}_1^{-1}\boldsymbol{f}_1^{(0)}$
(H)	$\boldsymbol{f}_1^{(0)^\dagger}\boldsymbol{\omega}_1^{-1}\boldsymbol{C}_{11}^{(2)}\boldsymbol{\omega}_1^{-1}\boldsymbol{C}_{11}^{(1)}\boldsymbol{\omega}_1^{-1}\boldsymbol{f}_1^{(0)}+\text{h.c.}$
(I)	$\boldsymbol{f}_1^{(0)^\dagger}\boldsymbol{\omega}_1^{-1}\boldsymbol{C}_{11}^{(1)}\boldsymbol{\omega}_1^{-1}\boldsymbol{C}_{11}^{(1)}\boldsymbol{\omega}_1^{-1}\boldsymbol{C}_{11}^{(1)}\boldsymbol{\omega}_1^{-1}\boldsymbol{f}_1^{(0)}$
(J)	$\boldsymbol{f}_2^{(2)^\dagger}\boldsymbol{\omega}_2^{-1}\boldsymbol{C}_{21}^{(1)}\boldsymbol{\omega}_1^{-1}\boldsymbol{f}_1^{(0)}+\text{h.c.}$
(K)	$\boldsymbol{f}_2^{(1)^\dagger}\boldsymbol{\omega}_2^{-1}\boldsymbol{C}_{22}^{(1)}\boldsymbol{\omega}_2^{-1}\boldsymbol{C}_{21}^{(1)}\boldsymbol{\omega}_1^{-1}\boldsymbol{f}_1^{(0)}+\text{h.c.}$
(L)	$\boldsymbol{f}_2^{(1)^\dagger}\boldsymbol{\omega}_2^{-1}\boldsymbol{C}_{21}^{(2)}\boldsymbol{\omega}_1^{-1}\boldsymbol{f}_1^{(0)}+\text{h.c.}$
(M)	$\boldsymbol{f}_2^{(1)^\dagger}\boldsymbol{\omega}_2^{-1}\boldsymbol{C}_{21}^{(1)}\boldsymbol{\omega}_1^{-1}\boldsymbol{f}_1^{(1)}+\text{h.c.}$
(N)	$\boldsymbol{f}_2^{(1)^\dagger}\boldsymbol{\omega}_2^{-1}\boldsymbol{C}_{21}^{(1)}\boldsymbol{\omega}_1^{-1}\boldsymbol{C}_{11}^{(1)}\boldsymbol{\omega}_1^{-1}\boldsymbol{f}_1^{(0)}+\text{h.c.}$
(O)	$\boldsymbol{f}_1^{(1)^\dagger}\boldsymbol{\omega}_1^{-1}\boldsymbol{C}_{12}^{(1)}\boldsymbol{\omega}_2^{-1}\boldsymbol{C}_{21}^{(1)}\boldsymbol{\omega}_1^{-1}\boldsymbol{f}_1^{(0)}+\text{h.c.}$
(P)	$\boldsymbol{f}_1^{(0)^\dagger}\boldsymbol{\omega}_1^{-1}\boldsymbol{C}_{12}^{(1)}\boldsymbol{\omega}_2^{-1}\boldsymbol{C}_{21}^{(2)}\boldsymbol{\omega}_1^{-1}\boldsymbol{f}_1^{(0)}+\text{h.c.}$
(Q)	$\boldsymbol{f}_1^{(0)^\dagger}\boldsymbol{\omega}_1^{-1}\boldsymbol{C}_{12}^{(1)}\boldsymbol{\omega}_2^{-1}\boldsymbol{C}_{21}^{(1)}\boldsymbol{\omega}_1^{-1}\boldsymbol{C}_{11}^{(1)}\boldsymbol{\omega}_1^{-1}\boldsymbol{f}_1^{(0)}+\text{h.c.}$
(R)	$\boldsymbol{f}_1^{(0)^\dagger}\boldsymbol{\omega}_1^{-1}\boldsymbol{C}_{12}^{(1)}\boldsymbol{\omega}_2^{-1}\boldsymbol{C}_{22}^{(1)}\boldsymbol{\omega}_2^{-1}\boldsymbol{C}_{21}^{(1)}\boldsymbol{\omega}_1^{-1}\boldsymbol{f}_1^{(1)}$
(S)	$\boldsymbol{f}_2^{(2)^\dagger}\boldsymbol{\omega}_2^{-1}\boldsymbol{f}_2^{(1)}+\text{h.c.}$
(T)	$\boldsymbol{f}_2^{(1)^\dagger}\boldsymbol{\omega}_2^{-1}\boldsymbol{C}_{22}^{(1)}\boldsymbol{\omega}_2^{-1}\boldsymbol{f}_2^{(1)}$

The basic step of generating and drawing the diagrams has been achieved with the help of a computer program based on a simple matrix representation of the diagrams. As briefly discussed in Appendix B, the matrix representation allows for a unique algorithmic treatment of the diagrams, guaranteeing in particular their completeness and correctness. The sorted matrices are read by a follow-up program[37] that transforms each matrix into a PostScript code and generates a graphic output, that is, a ''book'' of all 1380 diagrams. Moreover, the program prints the corresponding analytical expressions up to the sign and sorts the diagrams according to their integral type. As explained below, diagrams of the same integral type often have to be combined in the course of the ADC procedure.

Once the diagrams have been generated and drawn in an appropriate order, the ADC analysis is no longer an adamant endeavor. Many diagrams can be directly assigned to the algebraic terms of Table II, even without the need to write up the analytical expressions. The derivation of the new quantities listed above requires the inspection of relatively few ''key'' diagrams. The number of key diagrams determining the contributions $\boldsymbol{C}_{11}^{(3)}$, $\boldsymbol{C}_{12}^{(2)}$ and $\boldsymbol{C}_{22}^{(1)}$ is about 50. About 200 additional diagrams have to be inspected to specify also the

effective transition amplitudes $\boldsymbol{f}_1^{(3)}$ and $\boldsymbol{f}_2^{(2)}$. In Sec. III C the interested reader may find a brief survey of the third-order ADC analysis. The final expressions for $\boldsymbol{K}+\boldsymbol{C}$ are listed in Appendix C. A full list of the $\boldsymbol{f}$ expressions is available by request from the authors or can be downloaded from our website.[38]

C. Details of the third-order ADC analysis

In the following six paragraphs we take a closer look into the third-order ADC procedure. Let us note that a good deal of this section will be useful only for a reader interested in repeating the ADC(3) derivation. First we consider, in Secs. III C 1–III C 4 the treatment of different groups of diagrams. Then in Sec. III C 5 and Sec. III C 6, the perspective changes to the side of the ADC expressions. One may distinguish three groups of third-order diagrams, namely the diagrams (1)–(6), representing products $\boldsymbol{G}^{(0)}\boldsymbol{G}^{(3)}$ of a zeroth and a third-order one-particle Green's function; the diagrams (7)–(15) which are of the form $\boldsymbol{\Pi}^{(0)}\boldsymbol{C}^{(1)}\boldsymbol{\Pi}^{(2)}$ or $\boldsymbol{\Pi}^{(2)}\boldsymbol{C}^{(1)}\boldsymbol{\Pi}^{(0)}$; and finally the diagrams (16)–(23), characterized by a so called irreducible *p-h* vertex. In the latter groups one may note a topological similarity between the diagrams (16)–(19), (20) and (21), (22) and (23), respectively. As a separate special case we will consider the RPA diagram (7) in the beginning. As a common feature of all Feynman diagrams we note that the time orderings $9(a-f)$ and their counterparts $10(a-f)$ have the form of the ADC terms (A_1) and (A_2), respectively, in Table II. As a result there are $6\times 23 = 138$ trivial contributions to $\boldsymbol{f}_1^{(3)}$ which can be read off the diagrams in a straightforward way.

1. The RPA diagram

The 60 Goldstone diagrams associated with the RPA diagram (7) are shown in Fig. 4. As already mentioned, the ADC analysis of the time orderings $9(a-f)$ [and $10(a-f)$] is trivial leading to six distinct $\boldsymbol{f}_1^{(3)}$ contributions. The diagrams $(1a)-(8a)$ and in addition, $(5b)$, $(7b)$, $(6d)$, and $(8d)$ are readily identified as repetitive terms of the ADC expansion. For example, diagram $(7a)$ is of the form $\boldsymbol{f}_1^{(1)^\dagger}\boldsymbol{\omega}_1^{-1}\boldsymbol{f}_1^{(2)}$ [term (B_2) in Table II], where the $\boldsymbol{f}_1^{(2)}$ contribution is the one arising from the second-order diagrams (C11) and (C12).

For the remaining diagrams, things become somewhat more complex, as none of them fits individually to any of the ADC terms, and moreover, some parts of the repetitive terms (B), (C), (D), and (H) cannot readily be retrieved in the diagrammatic expressions. The latter applies to repetitions of the ''complex'' $\boldsymbol{C}_{11}^{(2)}$ and $\boldsymbol{f}_{11}^{(2)}$ contributions considered in Sec. III A, for which already at the second-order level no immediate one-to-one relation between diagrams and ADC terms could be established. In the following we describe one procedure how diagrams and complex repetitive terms (CRT) can be combined algebraically yielding quite simple expressions for $\boldsymbol{C}_{11}^{(3)}$ and $\boldsymbol{f}_1^{(3)}$. The question of uniqueness will be addressed further below.

1. First we consider diagrams $(1c)-(8c)$. Obviously, these diagrams have a common integral structure and, thus, can be combined. A simple way is to form $S_1=(1c)+(2c)+(3c)+(4c)$, $S_2=(5c)+(7c)$, and $S_3=(6c)+(8c)$. It is readily seen, that S_1 is of the form (G) specifying a $\boldsymbol{C}_{11}^{(3)}$ contribution; S_2 and S_3 correspond to the Hermitian conjugate pair (A_2) and (A_1), respectively, yielding an $\boldsymbol{f}_1^{(3)}$ contribution.

2. A common integral structure is found for diagrams $(1e)-(5e)$, $(7e)$, $(1b)$, and $(3b)$. One recipe is as follows. Form $S_1=(1e)+(2e)+(3e)+(4e)$, $S_2=(1b)+(3b)$, and compare S_1 and S_2 with the complex repetitive terms (H_2) and (C_2) where, of course, only the RPA contributions to $\boldsymbol{C}_{11}^{(2)}$ and $\boldsymbol{f}_1^{(2)}$ are to be considered. Straightforward algebra leads to an expression of the form (G) specifying another $\boldsymbol{C}_{11}^{(3)}$ contribution [which incidentally is one-half of what would result directly from (S_1)]. In an analogous way one can treat the diagrams $(1f)-(4f)$, $(1d)$, and $(2d)$, and the CRT's (H_1) and (C_1) yielding a Hermitian conjugate $\boldsymbol{C}_{11}^{(3)}$ contribution. The remaining diagrams, combined as $(5e)+(7e)$ and $(6f)+(8f)$ yield a $\boldsymbol{f}_1^{(3)}$ contribution according to (A_2) and (A_1), respectively.

3. There remain two more sets of diagrams with the same integral structure. For the first set we combine diagrams as follows. Form $S_1=(2b)+(4b)$, $S_2=(6b)+(8b)+(6e)+(8e)$, and compare S_1 and S_2 with the CRT contributions (B_2) and (D_1). Straightforward algebra leads to an expression of the form (A_2) specifying an $\boldsymbol{f}_1^{(3)}$ contribution. The corresponding Hermitian conjugate term of (A_1) form is obtained analogously from $(3d)$, $(4d)$, $(5d)$, $(7d)$, $(5f)$, and $(7f)$.

Herewith all Goldstone diagrams of the RPA diagram (7) (Fig. 4) have been exhausted. Altogether we have derived three $\boldsymbol{C}_{11}^{(3)}$ and three $\boldsymbol{f}_1^{(3)}$ contributions (plus six additional trivial $\boldsymbol{f}_1^{(3)}$ contributions).

The recipe used above for the ADC analysis of the RPA diagram (7) is not unique. The nonuniqueness encountered here is reflected by the fact that the ADC terms (A) and (G) may exchange contributions by applying partial fraction decomposition (PFD) and its inverse procedure. More specifically, nondiagonal contributions, say $\tilde{C}_{IJ}$ of $\boldsymbol{C}_{11}$ may be transferred to $\boldsymbol{f}_{11}$ as a result of PFD of (G), yielding the (anti-Hermitian) contributions

$$\tilde{f}_{IJ}=(K_I-K_J)^{-1}\tilde{C}_{IJ}, \tag{25}$$

in $\boldsymbol{f}_{11}$. Conversely, any anti-Hermitian contributions of $\boldsymbol{f}_{11}$ can be transferred into nondiagonal (but Hermitian) contributions of $\boldsymbol{C}_{11}$. Therefore, one arrives at a distinguished ADC scheme by imposing the symmetry condition

$$\boldsymbol{f}_{11}^\dagger=\boldsymbol{f}_{11}, \tag{26}$$

to the (1,1) block of $\boldsymbol{f}$. It should be clear that the differences in the results of the symmetrized and nonsymmetrized forms of the ADC(3) expressions are of fourth order.

2. Diagrams (8)–(15)

Obviously, the Feynman diagrams (8), (10), (12), and (14) can be constructed according to

$$D^{(x)}(\omega)=\boldsymbol{\Pi}^{(0)}(\omega)\boldsymbol{C}_{11}^{(1)}\boldsymbol{\Pi}^{(2,x)}(\omega), \tag{27}$$

as the products of the free (zeroth-order) propagator, the first-order secular matrix $\boldsymbol{C}_{11}^{(1)}$, and the second-order propa-

gator parts $\mathbf{\Pi}^{(2,x)}(\omega)$ where $x=A,B,D,E$ labels the second-order Feynman diagrams in Fig. 1, excluding the RPA diagram (C). Analogously, the Feynman diagrams (9), (11), (13), and (15) may be formulated as

$$D^{(x)}(\omega)=\mathbf{\Pi}^{(2,x)}(\omega)\boldsymbol{C}_{11}^{(1)}\mathbf{\Pi}^{(0)}(\omega), \tag{28}$$

where compared to Eq. (27), the order of the factors is interchanged. The total contribution of diagrams (8)–(15) plus the RPA diagram (7) can be written as

$$\begin{aligned}\sum_{h=7}^{15} D^{(h)}(\omega)=&\mathbf{\Pi}^{(0)}(\omega)\boldsymbol{C}_{11}^{(1)}\mathbf{\Pi}^{(2)}(\omega)\\&+\mathbf{\Pi}^{(2)}(\omega)\boldsymbol{C}_{11}^{(1)}\mathbf{\Pi}^{(0)}(\omega)\\&-\mathbf{\Pi}^{(1)}(\omega)\boldsymbol{C}_{11}^{(1)}\mathbf{\Pi}^{(1)}(\omega).\end{aligned} \tag{29}$$

Here the subtracted term on the right-hand-side corresponds to the RPA diagram (7) which is counted twice in the first two terms. Equation (29) offers an alternative route to the ADC analysis of diagrams (7)–(15). Instead of inspecting the associated Goldstone diagrams one can use the already available second-order forms for $\mathbf{\Pi}^{+}(\omega)$ and $\mathbf{\Pi}^{-}(\omega)$ in conjunction with the following obvious projection formula:

$$\mathbf{\Pi}^{+}(\omega)=\frac{1}{2\pi i}\oint\frac{\mathbf{\Pi}(\omega')}{\omega'-\omega-i\eta}d\omega'. \tag{30}$$

Here the contour integration is to be closed in the lower complex ω'-plane. We have used both the projection method and the Goldstone analysis for mutual checking.

In the following we return to the Goldstone analysis of diagrams (8)–(15). Let us first consider the somewhat simpler cases (12)–(15). Obviously (12) and (13), (14) and (15) form pairs of ''antipodes,'' that is, (13) and (15) are obtained by turning upside-down (12) and (14), respectively. The treatment of these four diagrams is essentially analogous, and we may, for example, consider the 60 time orderings of diagram (15) (labeled according to the convention explained in Sec. III B). As above we can disregard the 12 trivial $(A_{1,2})$ contributions. Further 12 diagrams, namely $(1a)$–$(4a)$, $(6a)$, $(8a)$, $(1d)$–$(4d)$, $(6d)$, and $(8d)$, can readily be identified as repetitive ADC terms. An additional eight diagrams can be directly assigned to one of the ADC terms: The four diagrams $(5a)$, $(5b)$, $(5d)$, and $(5f)$ give expressions of the form (J_2), while the diagrams $(7a)$, $(7b)$, $(7d)$, and $(7f)$ contribute to (S_2). In the (J_2) term the $\boldsymbol{f}_2^{(2)}$ contributions to be determined occur in conjunction with $\boldsymbol{C}_{12}^{(1)}$. As described in Sec. III C 5 one has to collect all (J_2) [or (J_1)] contributions in order to disentangle the desired $\boldsymbol{f}_2^{(2)}$ contributions from the known $\boldsymbol{C}_{12}^{(1)}$ expressions. Alternatively, one could use the (S_2) [or (S_1)] term.

The remaining 28 diagrams do not fit individually to ADC terms, but the appropriate combinations are rather obvious. Both $(1e)+(2e)+(3e)+(4e)$ and $(1c)+(2c)+(3c)+(4c)$ are of the form (G), yielding four $\boldsymbol{C}_{11}^{(3)}$ contributions. The combinations $(1b)+(3b)$ and $(1f)+(3f)$ contribute to (P_1), while $(2b)+(4b)$ and $(2f)+(4f)$ are of the form (L_1). In (P_1) and (L_1) the sought $\boldsymbol{C}_{21}^{(2)}$ contributions arise in conjunction with $\boldsymbol{C}_{12}^{(1)}$ and $\boldsymbol{f}_2^{(1)}$, respectively. As in the case of $\boldsymbol{C}_{21}^{(2)}$, one must collect either all (P_1) or all (L_1) contributions in order to deduce $\boldsymbol{f}_2^{(2)}$ (see Sec. III C 5). Of course, one may equally consider the h.c. terms (P_2) or (L_2). The remaining 12 diagrams can readily be combined pairwise: $(5c)+(7c)$, $(5e)+(7e)$, $(6b)+(8b)$, $(6c)+(8c)$, $(6e)+(8e)$, and $(6f)+(8f)$. Here the first two pairs contribute to (A_2), while the latter four pairs contribute to (A_1).

Now let us turn to the diagrams (8)–(11), for which the ADC analysis is somewhat more complicated because, like for diagram (7), complex repetitive terms [originating from the second-order diagrams (A) and (B)] have to be recovered. Note that diagrams (10) and (11) are ''antipodes'' to (9) and (8), respectively. As a representative let us consider the Goldstone diagrams of (9) (labeled according to the convention explained in Sec. III B). It may suffice to discuss only diagrams bringing up new features, that is here, the 20 diagrams $(1c)$–$(1f)$, ..., $(4c)$–$(4f)$, $(5c)$, $(5e)$, $(7c)$, and $(7e)$. The common integral structure suggests to combine diagrams $(1f)$–$(4f)$, $(1d)$, and $(2d)$. Forming $S_1=(1f)+(2f)+(3f)+(4f)$ and $S_2=(1d)+(2d)$ one gets readily rid of the $3p$-$3h$ denominator ω_6^{-1}. Now one can compare S_1 and S_2 with the CRT's (H_1) and (C_1), where only the $\boldsymbol{C}_{11}^{(2)}$ and $\boldsymbol{f}_1^{(2)}$ contributions of the second-order diagram (A) are taken into account. The result is an expression of type (G) specifying a $\boldsymbol{C}_{11}^{(3)}$ contribution. In a similar way one obtains a $\boldsymbol{f}_1^{(3)}$ contribution by comparing $(3d)+(4d)$ with the appropriate CRT contributions of the type (D_2) and (B_1). For the combination $(1c)+(3c)+(5c)$ straightforward algebra yields an expression of form (G) from which one deduces a $\boldsymbol{C}_{11}^{(3)}$ contribution. In a similar way one obtains an (A_1) term from $(2c)+(4c)+(7c)$, specifying a $\boldsymbol{f}_1^{(3)}$ contribution. An analogous procedure applies to the diagrams $(1e)$–$(5e)$ and $(7e)$.

3. Diagrams (16)–(23)

After the cases considered so far, the ADC analysis of diagrams (16)–(23) is rather simple. There are no repetitive terms, and the only new feature is the occurrence of various $\boldsymbol{C}_{22}^{(1)}$ contributions. However, here the assignment of diagrams and ADC terms is straightforward. Moreover, the $\boldsymbol{C}_{22}^{(1)}$ expressions may be determined directly without the need of inspecting diagrams (see Sec. III C 6). Let us take a brief look to one of these diagrams, say to (22). The 12 Goldstone diagrams $(1a)$–$(4a)$, $(1b)$–$(4b)$, and $(1e)$–$(4e)$ correspond to $\boldsymbol{C}_{22}^{(1)}$ terms in one of the forms (K), (R), or (T). The combination of $(1f)$–$(4f)$ yields a $\boldsymbol{C}_{11}^{(3)}$ contribution according to term (G). Following the procedure described in the case of Feynman diagram (15), the diagrams $(1c)$–$(4c)$ and $(1d)$–$(4d)$ can be rewritten in the form of (P) and (L) terms, bearing information required to determine $\boldsymbol{C}_{12}^{(2)}$. In the same way as described for diagrams (8)–(15) the remaining diagrams contribute to terms (S), (J), or (A) specifying $\boldsymbol{f}_1^{(3)}$ and $\boldsymbol{f}_2^{(2)}$ contributions.

4. Diagrams (1)–(6)

This class of diagrams is a special case of contributions that in time representation are given by a product of two oppositely directed one-particle Green's functions (GF):

$$\tilde{\Pi}_{pq,rs}(t,t')=(-i)G_{pr}(t,t')G_{sq}(t',t), \tag{31}$$

Here the factor $(-i)$ is needed to reconcile the phase convention of the one-particle Green's functions with that of the polarization propagator. After Fourier transformation to energy representation Eq. (31) takes on the form of a convolution integral

$$\tilde{\Pi}_{pq,rs}(\omega)=\frac{1}{2\pi i}\int d\omega_1 G_{pr}(\omega_1)G_{pr}(\omega_1-\omega). \tag{32}$$

The simple product form of the diagrams (1)–(6), in which the third-order GF-parts $G^{(3)+}$,$G^{(3)-}$ are combined with the zeroth-order GF parts $G^{(0)-}$ and $G^{(0)+}$, respectively, suggests to exploit the recently established third-order ADC schemes for $\boldsymbol{G}^{-}$ (and $\boldsymbol{G}^{+}$).[39] Obviously, diagrams (1)–(3) can be combined according to

$$\begin{aligned}\tilde{\Pi}_{pk,rk'}(\omega)&=\frac{1}{2\pi i}\int d\omega_1 G^{(3)+}_{pr}(\omega_1)G^{(0)-}_{k'k}(\omega_1-\omega)\\&=\delta_{kk'}G^{(3)+}_{pr}(\omega+\epsilon_k).\end{aligned} \tag{33}$$

Analogously we find

$$\begin{aligned}\tilde{\Pi}_{aq,a's}(\omega)&=\frac{1}{2\pi i}\int d\omega_1 G^{(0)+}_{aa'}(\omega_1)G^{(3)-}_{sq}(\omega_1-\omega)\\&=(-1)\,\delta_{aa'}G^{(3)-}_{sq}(\epsilon_a-\omega),\end{aligned} \tag{34}$$

for diagrams (4)–(6). Inserting now the third-order ADC expressions for $\boldsymbol{G}^{(3)+}$ and $\boldsymbol{G}^{(3)-}$ as given in Ref. 39 yields readily the corresponding ADC terms for the polarization propagator. One should note that here only the nine terms [(A), (G), (J)–(L), (P), (R)–(T)] of Table II come into play, namely those without a $\boldsymbol{f}_1^{(1)}$ or $\boldsymbol{C}_{11}^{(1)}$ constituent. For the $\boldsymbol{C}_{11}^{(3)}$ and $\boldsymbol{f}_1^{(3)}$ contributions, the final expressions can directly be inferred from the $\boldsymbol{G}^{+}$ and $\boldsymbol{G}^{-}$ results. For example, the $\boldsymbol{C}_{11}^{(3)}$ contribution arising from diagrams (1)–(6) is simply given by

$$\tilde{C}^{(3)}_{ak,a'k'}=\delta_{aa'}(-1)C^{(3)-}_{kk'}+\delta_{kk'}C^{(3)+}_{aa'}, \tag{35}$$

where $C^{(3)-}_{kk'}$ and $C^{(3)+}_{aa'}$ are specified by Eqs. (A5)–(A9) and (B9) in Ref. 39. Of course, one may as well resort to the Goldstone analysis of diagrams (1)–(6). The Goldstone diagrams are obtained by a trivial extension of the diagrams for $\boldsymbol{G}^{(3)+}$ and $\boldsymbol{G}^{(3)-}$, respectively.

5. Derivation of $\boldsymbol{C}_{12}^{(2)}$ and $\boldsymbol{f}^{(2)}$

To determine the second-order contributions to $\boldsymbol{C}_{12}$ one may consider all (P_2) contributions and compare them to the general form

$$\begin{aligned}\sum_{a'b'k'l'}&(\omega-\epsilon_a+\epsilon_k)^{-1}C^{(2)}_{ak,a'b'k'l'}(\omega-\epsilon_{a'}-\epsilon_{b'}+\epsilon_k\\&+\epsilon_{k'})^{-1}C^{(1)}_{a'b'k'l',a''k''}(\omega-\epsilon_{a''}+\epsilon_{k''})^{-1},\end{aligned} \tag{36}$$

where one has to insert the given first order expression for $C^{(1)}_{a'b'k'l',a''k''}$ [see Eq. (C38)]. This allows one to deduce the constituents of $\boldsymbol{C}_{21}^{(2)}$ without major difficulties. One may distinguish contributions to $C^{(2)}_{ak,a'b'k'l'}$ with the Kronecker symbol $\delta_{aa'}$, with the Kronecker symbol $\delta_{kk'}$, and without any Kronecker symbol. The diagrams contributing to (P_2) may be distinguished according to these three types

$\delta_{aa'}$: (4),(5),(17),(19–21),(23)

$\delta_{kk'}$: (1),(2),(16),(18),(20–22)

none: (8),(10),(12)$(\times 2)$,(14)$(\times 2)$.

Note that diagrams (12) and (14) give two (P_2) contributions each. As the next step, the preliminary total expression for $C^{(2)}_{ak,a'b'k'l'}$ has to be antisymmetrized with respect to a',b' and k',l', respectively. The antisymmetrized expressions can then be verified by inserting them into Eq. (36) which must recover the 20 original (P_2) contributions. Alternatively, one could have used the terms (P_1), (L_1), or (L_2). In a similar way, $\boldsymbol{f}_2^{(2)}$ can be deduced from any set of (S_1),(S_2),(J_1), or (J_2) contributions.

6. Derivation of $\boldsymbol{C}_{22}^{(1)}$

The diagrammatic derivation of $\boldsymbol{C}_{22}^{(1)}$ using either (R), (T), or (K) contributions poses no difficulties. The corresponding Goldstone diagrams of the Feynman diagrams (1), (2), (4), (5), (16)–(23) can directly be assigned to the algebraic terms. However, it is not necessary to refer to diagrams, because the first-order contribution to $\boldsymbol{C}_{22}^{(1)}$ is given by the well-known configuration interaction (CI) expression

$$C^{(1)}_{abkl,a'b'k'l'}=\langle\Phi_{abkl}|\hat{H}-E_0(1)|\Phi_{a'b'k'l'}\rangle. \tag{37}$$

Here $|\Phi_{abkl}\rangle=c_a^\dagger c_b^\dagger c_k c_l|\Phi_0\rangle (a<b,k<l)$ is a doubly exited CI configuration and $E_0(1)=\langle\Phi_0|\hat{H}|\Phi_0\rangle$ is the first-order ground-state energy. As an obvious extension to the ADC(2) scheme, the first-order $\boldsymbol{C}_{22}$ block has been considered previously.[11]

IV. MISCELLANEOUS ASPECTS OF THE ADC POLARIZATION PROPAGATOR FORMULATION

In the following three subsections we will discuss briefly some consequences of the ADC approach to the polarization propagator. First we consider physical quantities related to the p-h density matrix. As important checks for the quality of a computional scheme, the dipole sum rule and the equivalence of the length and velocity forms of the transition moment will be considered in Sec. IV B. Finally, in Sec. IV C the ADC reformulation of the RPA equations will briefly be addressed.

A. Generalized spectral moments and the particle-hole density matrix

A quantity related to the polarization propagator is the p-h density matrix.

$$\rho^{ph}_{rs,r's'}=\langle\Psi_0|c_s^\dagger c_r c_{r'}^\dagger c_{s'}|\Psi_0\rangle-\rho_{sr}\rho_{r's'}, \tag{38}$$

where $\rho_{uv}=\langle\Psi_0|c_u^\dagger c_v|\Psi_0\rangle$ denotes the familiar one-particle density matrix. Obviously $\boldsymbol{\rho^{ph}}$ can be obtained from $\mathbf{\Pi}^+$ (or $\mathbf{\Pi}$) by the contour integral

$$\boldsymbol{\rho^{ph}}=-\frac{1}{2\pi i}\oint \mathbf{\Pi}^+(\omega)d\omega, \tag{39}$$

where the integration path closes in the lower complex ω-plane. Inserting for $\mathbf{\Pi}^+(\omega)$ the ADC representation [Eq. (8)] yields the relation

$$\boldsymbol{\rho^{ph}}=\boldsymbol{f}^\dagger\boldsymbol{f}. \tag{40}$$

The p-h density matrix is a special case ($m=0$) of the following generalized spectral moments:

$$S^{(m)}_{rs,r's'}=\langle\Psi_0|c_s^\dagger c_r(\hat{H}-E_0)^m\hat{Q}_0 c_{r'}^\dagger c_{s'}|\Psi_0\rangle$$
$$=\sum_{n\neq 0}(E_n-E_0)^m\langle\Psi_0|c_s^\dagger c_r|\Psi_n\rangle\langle\Psi_n|c_{r'}^\dagger c_{s'}|\Psi_0\rangle. \tag{41}$$

Here the second line follows by inserting the complete set of excited states $|\Psi_n\rangle$. One may readily derive the relationship

$$S^{(m)}=\boldsymbol{f}^\dagger(\mathbf{K}+\mathbf{C})^m\boldsymbol{f}, \tag{42}$$

by inserting into Eq. (41) instead of the exact states the intermediate states $|\tilde{\Psi}_J\rangle$ of the ADC representation [Eq. (8)]. One may note that $S^{(m)}$ can be calculated directly from $\boldsymbol{f}$ and $\boldsymbol{K}+\boldsymbol{C}$ without the need to diagonalize the secular matrix $\boldsymbol{K}+\boldsymbol{C}$. The relationship

$$\gamma_{pq,p'q'}=-\rho^{ph}_{q'p,qp'}+\delta_{qq'}\rho_{pp'}+\rho_{pq'}\rho_{qp'}, \tag{43}$$

between the p-h density and the more familiar reduced two-particle density matrix

$$\gamma_{pq,p'q'}=\langle\Psi_0|c_p^\dagger c_q^\dagger c_{q'}c_{p'}|\Psi_0\rangle, \tag{44}$$

shows that $\boldsymbol{\rho^{ph}}$ is not so well suited for representing the ground-state expectation value of a two-particle operator. As is well known,[1] a more natural relationship is found for the ground-state expectation value of products of two single-particle operators, say $\hat{A}=\Sigma A_{rs}c_r^\dagger c_s$ and $\hat{B}=\Sigma B_{rs}c_r^\dagger c_s$. In particular the compact relation

$$\langle\Psi_0|(\hat{A}-\langle A\rangle)(\hat{B}-\langle B\rangle)|\Psi_0\rangle=\boldsymbol{A}^\dagger\boldsymbol{\rho^{ph}}\boldsymbol{B}=\boldsymbol{A}^\dagger\boldsymbol{f}^\dagger\boldsymbol{f}\boldsymbol{B}, \tag{45}$$

is obtained for the product of ''deviation'' operators $\hat{A}-\langle A\rangle$ and $\hat{B}-\langle B\rangle$. Here $\langle X\rangle=\langle\Psi_0|\hat{X}|\Psi_0\rangle$ and $\boldsymbol{A}(\boldsymbol{B})$ is the matrix of single-particle integrals $A_{rs}(B_{rs})$. Note that for $\hat{A}=\hat{B}$, Eq. (45) describes the ground-state fluctuation of a single-particle operator.

An interesting conclusion follows for the choice:

$$\hat{B}=\hat{N}=\sum_r c_r^\dagger c_r. \tag{46}$$

Since $|\Psi_0\rangle$ is an eigenfunction of the particle number operator $\hat{N}$, the deviation operator product has a vanishing expectation value, that is

$$\sum_J\left(\sum_{rs}A^*_{rs}f^*_{J,rs}\right)\left(\sum_p f_{J,pp}\right)=0, \tag{47}$$

for arbitrary matrix elements A_{rs}. The immediate consequence is that

$$\sum_p f_{J,pp}=0, \tag{48}$$

for any configuration J. Of course this result could have been inferred directly from noting that

$$\sum_p f_{J,pp}=\langle\tilde{\Psi}_J|\hat{N}|\Psi_0\rangle=0, \tag{49}$$

as the intermediate states $|\tilde{\Psi}_J\rangle$ are orthogonal to the exact ground state. The relation (48) holds in any order of perturbation theory and, moreover, does not depend on the underlying single particle basis set. It may serve as an important check of the complex expressions derived for $\boldsymbol{f}$. Unfortunately, only contributions with pp or hh index pairs are concerned.

B. The dipole sum rule and the equivalence of length and velocity form of the transition moments

The well-known Thomas–Reiche–Kuhn (TRK) or dipole sum rule states that the first moment

$$S_z^{(1)}=\sum_n(E_n-E_0)|\langle\Psi_n|\hat{Z}|\Psi_0\rangle|^2=\tfrac{1}{2}N, \tag{50}$$

of the excitation spectrum for the z component of the dipole operator

$$\hat{Z}=\sum_{i=1}^N\hat{z}^{(i)}=\sum_{i=1}^N d^{(z)}_{rs}c_r^\dagger c_s, \tag{51}$$

equals one-half of the electron number N. This relation follows from the identity of the explicit form and the double commutator expression

$$S_z^{(1)}=\tfrac{1}{2}\langle\Psi_0|[\hat{Z},[\hat{H},\hat{Z}]]|\Psi_0\rangle. \tag{52}$$

Analogous relations hold for the x and y components. The ADC formulation [Eq. (42)] for the generalized transition moments can be readily transferred to $S_z^{(1)}$ yielding

$$S_z^{(1)}=\underline{F}(z)^\dagger(\boldsymbol{K}+\boldsymbol{C})\underline{F}(z)=\tfrac{1}{2}N, \tag{53}$$

where $\underline{F}(z)$ is the (column) vector of effective transition moments [see Eq. (17)]

$$F_J^{(z)}=\sum_{r,s}f_{J,rs}d^{(z)}_{rs}, \tag{54}$$

for the transition operator $\hat{Z}$. Equation (53) offers an important test for the quality of the computational scheme. However, deviations from the exact result arise not only from using approximative ADC schemes, but also from the incompleteness of the underlying single-particle basis. For a dis-

cussion of how these two factors can be disentangled to a certain extent, the reader is referred to Ref. 14.

Another significant quality test is the agreement between the dipole length (L) and dipole velocity (V) forms of the transition moments. As is well known, the following identity holds for the exact ground and excited states:

$$(E_m - E_0)\langle \Psi_m|\hat{Z}|\Psi_0\rangle = -i\langle \Psi_m|\hat{P}_z|\Psi_0\rangle. \tag{55}$$

Here $\hat{P}_z$ is the z component of the momentum operator. The expressions on the left- and right-hand-side are referred to as (L) and (V) form, respectively, of the transition moment. In the ADC formulation the left-hand-side of Eq. (55) can be written as

$$(E_m - E_0)\langle \Psi_m|\hat{Z}|\Psi_0\rangle = \underline{Y}^{(m)\dagger}(\boldsymbol{K}+\boldsymbol{C})\underline{F}(z), \tag{56}$$

while the (V) transition moment is given by

$$\langle \Psi_m|\hat{P}_z|\Psi_0\rangle = \underline{Y}^{(m)\dagger}\underline{F}(p_z). \tag{57}$$

Here $\underline{F}(p_z)$ is the vector of effective transition moments [Eq. (17)] for $\hat{P}_z$. By abstracting the scalar product with the eigenvector $\underline{Y}^{(m)\dagger}$ both in Eqs. (56) and (57), one yields the general identity

$$(\boldsymbol{K}+\boldsymbol{C})\underline{F}(z) = -i\underline{F}(p_z), \tag{58}$$

which is no longer restricted to a particular transition.[14] As in the dipole sum rule, deviations from this relation reflect both the approximation level of the ADC scheme and basis set insufficiencies.

In a similar way the static and dynamic (dipole) polarizabilities can be expressed in terms of ADC quantities. For details the reader is referred to a forthcoming paper.

C. The random-phase approximation (RPA) in the ADC form

As is well known, the subset of Feynman diagrams constituted by diagrams (0), (1), (C) in Fig. 1, diagram (7) in Fig. 3 and similarly constructed diagrams of order $n = 4,5,6,\ldots$ can be summed exactly leading to the famous random-phase approximation (RPA) for the polarization propagator.[1] The RPA is an example of an infinite, though partial summation of Feynman diagrams. Obviously, the error introduced by omitting diagrams is of second order, which severely restricts the usefulness of the RPA in atomic and molecular applications.

It should be clear that the ADC procedure applied here to the full polarization propagator could have been specialized as well to the class of RPA diagrams. As described in Ref. 40 this leads to an ADC representation of the RPA polarization propagator part according to

$$\boldsymbol{\Pi}^{\mathrm{RPA}(+)} = \boldsymbol{f}^{\mathrm{RPA}\dagger}(\omega\hat{\mathbf{1}} - (\boldsymbol{K}+\boldsymbol{C})^{\mathrm{RPA}})^{-1}\boldsymbol{f}^{\mathrm{RPA}}, \tag{59}$$

where the configuration space of the secular matrix $(\boldsymbol{K}+\boldsymbol{C})^{\mathrm{RPA}}$ is spanned by the manifold of single excitations $\{J\} = \{aj\}$. The second index pair (rs) of the effective transition amplitudes $f_{J,rs}$ is restricted to p-h and h-p pairs. The ADC reformulation of the RPA is of some interest as it splits the RPA pseudo-eigenvalue problem into two equivalent and, in general, Hermitian eigenvalue problems of half dimension. In Ref. 40 the secular matrix $\boldsymbol{C}^{\mathrm{RPA}}$ and the effective transition moments $\boldsymbol{f}^{\mathrm{RPA}}$ have been specified through second order. Using the results of the present ADC analysis for the RPA diagram (7) in Fig. 2 the RPA–ADC scheme can be extended to third order. The third-order contributions to $\boldsymbol{C}^{\mathrm{RPA}}$ are specified in Eqs. (C21) and (C22).

V. DISCUSSION

A. General ADC properties

The third-order ADC procedure for the polarization propagator has lead to a structurally simple extension of the existing ADC(2) scheme. In both the ADC(2) and ADC(3) methods the (vertical) electronic excitation energies are given directly by the eigenvalues of a Hermitian secular matrix $\boldsymbol{K}+\boldsymbol{C}$ defined with respect to a configuration space of p-h (single) and $2p$-$2h$ (double) excitations (see Fig. 5). The corresponding transition moments are obtained as the dot products of the respective eigenvectors and a vector $\boldsymbol{f}$ of effective transition amplitudes. Both the matrix elements of $\boldsymbol{K}+\boldsymbol{C}$ and $\boldsymbol{f}$ are given by first-, second-, and third-order perturbation expansions of Rayleigh–Schrödinger type. The ADC(3) method extends the perturbation-theoretical consistency to third order for the single excitations and to first order for the double excitations, allowing for higher accuracy than at the second-order level though at substantially higher computational cost.

The ADC computational schemes combine matrix diagonalization and perturbation theory (''as little diagonalization as necessary, as much perturbation theory as possible''). Three basic properties, referred to as *regularity*, *compactness*, and *separability* establish the usefulness of these schemes:[22,41,42]

(i) *Regularity* means that the perturbation expansions for $\boldsymbol{K}+\boldsymbol{C}$ and $\boldsymbol{f}$ behave essentially like the Rayleigh–Schrödinger series for E_0 and $|\Psi_0\rangle$, respectively. There are no ''dangerous denominators'' provided there is a finite energy gap between the occupied and virtual ground-state orbitals.

(ii) The explicit configuration spaces are smaller (more *compact*) than those of comparable CI expansions. For example, a consistent second- or third-order CI treatment of single excitations would require to include $3p$-$3h$ configurations. By contrast, the explicit ADC(3) configuration space extends only to the $2p$-$2h$ excitation class.

(iii) The ADC equations are *separable*, that is, local excitations in a system of noninteracting (separate) fragments decouple strictly from nonlocal excitations. This guarantees size-intensive results, i.e., neither excitation energies nor transition moments of a (local) fragment excitation depend on whether the method is applied to the fragment or to the entire system.

While combination of perturbation theory and secular equations is found also in the EOM/superoperator schemes such as the SOPPA method,[9,12,13] the latter schemes differ from the ADC approach in two essential points: The EOM secular equations are of the non-Hermitian RPA type, and the explicit secular configuration spaces are twice as large as in the ADC case, as they comprise in addition to the physical

excitations, e.g., p-h and $2p$-$2h$ excitations, also the corresponding unphysical excitations, that is, h-p and $2h$-$2p$ excitations in the given example. For a discussion of the compactness and separability properties of the EOM schemes the reader is referred to Mertins *et al.*[43]

It should be noted that the explicit ADC(3) expressions reflect the symmetry properties of the Hamiltonian. As a result, the ADC secular equations decouple with respect to different irreducible representations of the underlying symmetry group. In particular, spin-free working equations for singlet and triplet excitations can readily be derived for a spin-independent Hamiltonian, using standard techniques of tensorial analysis (see, for example, Ref. 14).

B. Comparison to CC methods

Both the ADC schemes and the various CC based methods can be discussed in the framework of a general concept referred to as intermediate state representations (ISR).[22] In the ADC case we recall that the secular equations could have been obtained directly as the representation of the (shifted) Hamiltonian $\hat{H}-E_0$

$$(\boldsymbol{K}+\boldsymbol{C})_{IJ}=\langle\tilde{\Psi}_I|\hat{H}-E_0|\tilde{\Psi}_J\rangle, \tag{60}$$

and the generalized transition operator

$$f_{J,rs}=\langle\tilde{\Psi}_J|c_r^\dagger c_s|\Psi_0\rangle, \tag{61}$$

with respect to a set of ''intermediate'' states $|\tilde{\Psi}_J\rangle$. These intermediate states are constructed from a set of ''correlated excited (CE) states''

$$|\Psi_J^0\rangle=\hat{C}_J|\Psi_0\rangle, \tag{62}$$

where

$$\{\hat{C}_J\}\equiv\{c_a^\dagger c_k;c_a^\dagger c_b^\dagger c_k c_l,a<b,k<l;\ldots\}, \tag{63}$$

is the manifold of physical excitation operators, by successive Gram–Schmidt orthogonalization of the p-h, $2p$-$2h$, ..., excitation classes. As a zeroth excitation class the exact ground-state $|\Psi_0\rangle$ may be incorporated so that the resulting intermediate states are orthogonal to $|\Psi_0\rangle$,

$$\langle\tilde{\Psi}_J|\Psi_0\rangle=0.$$

As shown in Refs. 22, 41, and 42 the representation based on these ''excitation class orthonormalized (ECO)'' intermediate states has the basic properties of regularity, compactness, and separability which establishes the equivalence of the ADC and ECO-ISR formulation. Here the role of the orthonormalization procedure is essential. Using symmetric orthonormalization instead of the ECO Gram–Schmidt procedure would not lead to a compact and separable representation. Explicit closed-form expressions for the blocks of $\boldsymbol{K}+\boldsymbol{C}$ and $\boldsymbol{f}$ for the first three excitation classes have been given in Ref. 41. This provides an alternative approach for deriving perturbation expansions for the matrix elements of $\boldsymbol{K}+\boldsymbol{C}$ and $\boldsymbol{f}$, namely by using perturbation theory for $|\Psi_0\rangle$ in the closed form expressions. In practice, however, it turns out that the original diagrammatic procedure pursued above is still a much simpler and safer way for deriving the explicit working equations.

As the main representative of the CC methods we will briefly consider the biorthogonal coupled cluster (bCC) representation used, for example, in the CCLR theory of Koch and Jørgensen[29,30] and in the EOM-CC method as formulated by Stanton and Bartlett.[35] For a more comprehensive discussion the reader is referred to Ref. 22. The bCC formulation is based on a mixed representation of $\hat{H}-E_0$ in terms of two sets of states, namely the CE states

$$|\Psi_J^0\rangle=\hat{C}_J\exp(\hat{T})|\Phi_0\rangle=\exp(\hat{T})\hat{C}_J|\Phi_0\rangle, \tag{64}$$

on the right-hand-side, and the associated biorthogonal states

$$\langle\Psi_I^\perp|=\langle\Phi_0|\hat{C}_I^\dagger\exp(-\hat{T}), \tag{65}$$

on the left-hand-side. Here $\hat{C}_I$ denote the physical excitation operators as specified in Eq. (63). The familiar CC parametrization

$$|\Psi_0^{\mathrm{CC}}\rangle=\exp(\hat{T})|\Phi_0\rangle, \tag{66}$$

is used for the ground state; here $|\Phi_0\rangle$ denotes the HF ground state. The cluster operator

$$\hat{T}=\sum_I t_I\hat{C}_I,$$

is given as a sum of physical excitation operators and, thus, $\hat{T}$ commutes with any $\hat{C}_J$. The bCC representation leads to the following non-Hermitian secular matrix $\boldsymbol{M}$:

$$\begin{aligned}\boldsymbol{M}_{IJ}&=\langle\Psi_I^\perp|\hat{H}-E_0|\Psi_J^0\rangle\\&=\langle\Phi_0|\hat{C}_I^\dagger\exp(-\hat{T})[\hat{H},\hat{C}_J]\exp(\hat{T})|\Phi_0\rangle.\end{aligned} \tag{67}$$

The excitation energies ω_m are obtained either from the right or the left eigenvalue problem

$$\begin{aligned}&\boldsymbol{MX}=\boldsymbol{X\Omega},\\&\boldsymbol{Y}^\dagger\boldsymbol{M}=\boldsymbol{\Omega Y}^\dagger,\end{aligned} \tag{68}$$

where ω is the diagonal matrix of eigenvalues ω_m, and $\boldsymbol{X}(\boldsymbol{Y})$ denotes the matrix of right (left) eigenvectors. The two versions of the secular equations can be combined according to

$$\boldsymbol{Y}^\dagger\boldsymbol{MX}=\boldsymbol{\Omega},\quad\boldsymbol{Y}^\dagger\boldsymbol{X}=\boldsymbol{1}, \tag{69}$$

so that the right and left eigenvectors are biorthonormal but in general not normalized. The corresponding right and left eigenstates can be written as follows:

$$\begin{aligned}|\Psi_n\rangle&=\sum_I X_{In}|\Psi_I^0\rangle,\\\langle\overline{\Psi}_n|&=\sum_I Y_{In}^*\langle\Psi_I^\perp|.\end{aligned} \tag{70}$$

It should be noted that the excitation energies are not affected in the extended representation $\boldsymbol{M}'$ including the exact and the HF ground state, $|\Psi_0^{CC}\rangle$ and $|\Phi_0\rangle$, respectively

$$\boldsymbol{M}'=\begin{pmatrix}0&\boldsymbol{v}\\\boldsymbol{0}&\boldsymbol{M}\end{pmatrix}. \tag{71}$$

	$1p$-$1h$	$2p$-$2h$	$3p$-$3h$	$4p$-$4h$	$5p$-$5h$	...
$1p$-$1h$	0	1	2	3	4	...
$2p$-$2h$	1	0	1	2	3	...
$3p$-$3h$	2	1	0	1	2	...
$4p$-$4h$	3	2	1	0	1	...
$5p$-$5h$	4	3	2	1	0	...
⋮	⋮	⋮	⋮	⋮	⋮	⋮

(a)

	$1p$-$1h$	$2p$-$2h$	$3p$-$3h$	$4p$-$4h$	$5p$-$5h$	...
$1p$-$1h$	0	1	1	–	–	...
$2p$-$2h$	1	0	1	1	–	...
$3p$-$3h$	2	1	0	1	1	...
$4p$-$4h$	3	2	1	0	1	...
$5p$-$5h$	4	3	2	1	0	...
⋮	⋮	⋮	⋮	⋮	⋮	⋮

(b)

FIG. 6. Order relations of the secular matrix blocks in the ADC (or ECO-IS) representation (a) and in the biorthogonal coupled cluster (BCC) representation (b). The numbers in the blocks indicate the lowest nonvanishing order of perturbation theory; empty blocks vanish.

Here $\boldsymbol{v}$ is a row vector with the elements

$$v_I=\langle\Phi_0|[\hat{H},\hat{C}_I]\exp(\hat{T})|\Phi_0\rangle. \tag{72}$$

The left eigenvector of $\boldsymbol{M}'$ associated with the ground state ($\omega_0=0$)

$$\underline{Y}_0'=\begin{pmatrix}1\\ \underline{Y}_0\end{pmatrix}$$

where

$$\underline{Y}_0^{\dagger}=-\boldsymbol{v}\boldsymbol{M}^{-1}, \tag{73}$$

can be used to form a representation of the ground state

$$\langle\overline{\Psi}_0|=\langle\Phi_0|+\sum_I Y_{I0}^{*}\langle\Psi_I^{\perp}|, \tag{74}$$

in terms of the biorthogonal states. This is the ''dual'' state designated $\langle\Lambda|$ in the work of Koch and Jørgensen;[29,30] the row vector $\boldsymbol{v}$ is their vector $\boldsymbol{\eta}$.

The analysis of the perturbation-theoretical (PT) consistency of approximative methods, obtained, for example, by truncating the configuration space, has to be based on the order relations (that is the lowest nonvanishing PT order) of the blocks of the secular matrix. In Fig. 6 we compare the order relations of the ADC (ECO-ISR) and bCC secular matrices as derived in Refs. 22 and 36. While the ADC secular matrix fulfills the so-called canonical order relations, the bCC matrix $\boldsymbol{M}$ is canonical in the lower triangular part, but has the typical CI structure in the upper triangular part. (Note that in the derivation of Ref. 22, the bCC order relations could have been made more stringent [as in Fig. 6(b)] by exploiting the fact, that $\hat{T}$ is a physical operator.) As a result, the bCC compactness properties are weaker than those of the ADC. This means, for example, that the usual truncation of the configuration space beyond the p-h and $2p$-$2h$ excitation manifold, allows for third-order consistency in the ADC case, but only for a consistent second-order description of the excitation energies in the truncated bCC scheme.

The second essential property, the size intensivity of the results, is fulfilled for the excitation energies as a consequence of the separability of the characteristic polynomial (see Refs. 22 and 29).

The CCLR and EOM-CC methods differ in the treatment of spectral intensities. In the latter method the squared transition moments

$$|T_n|^2=\alpha\langle\overline{\Psi}_n|\hat{D}|\Psi_0^{\mathrm{CC}}\rangle\langle\Psi_0^{\mathrm{CC}}|\hat{D}|\Psi_n\rangle, \tag{75}$$

are obtained as the product of a left and a right transition moment

$$\begin{aligned}T_n^{(l)}&=\langle\overline{\Psi}_n|\hat{D}|\Psi_0^{\mathrm{CC}}\rangle,\\ T_n^{(r)}&=\langle\Psi_0^{\mathrm{CC}}|\hat{D}|\Psi_n\rangle.\end{aligned} \tag{76}$$

The normalization constant $\alpha=\langle\Psi_0^{\mathrm{CC}}|\Psi_0^{\mathrm{CC}}\rangle^{-1}$ corrects for the intermediate normalization of $|\Psi_0^{\mathrm{CC}}\rangle$. Here and in the following we assume that $|\Psi_0^{\mathrm{CC}}\rangle$ and $|\Psi_n\rangle$ differ by symmetry so that there is no admixture of $|\Psi_0^{\mathrm{CC}}\rangle$ in $|\Psi_n\rangle$ of Eq. (70). While the left transition moment $T_n^{(l)}$ is separable (size-intensive), the right transition moment does not have this property.[22,44] The weaker compactness property leads to a second-order consistency of both $T_n^{(r)}$ and $T_n^{(l)}$ (for a single excitation) in the truncated bCC(SD) method. In the CCLR formulation of Koch and Jørgensen[29] one keeps the left transition moment as it is but sets out from the following form for the right transition moment

$$T_n^{(r)}=\langle\overline{\Psi}_0|\hat{D}|\Psi_n\rangle, \tag{77}$$

where $\langle\overline{\Psi}_0|$ is the dual ground state of Eq. (74). Since $\langle\overline{\Psi}_0|\Psi_0\rangle=1$ the normalization constant in Eq. (75) can be skipped ($\alpha=1$). The lack of separability is circumvented by rewriting $T_n^{(r)}$ as follows:

$$\begin{aligned}T_n^{(r)}&=\langle\overline{\Psi}_0|\hat{D}\hat{C}_n|\Psi_0^{\mathrm{CC}}\rangle\\ &=\langle\overline{\Psi}_0|[\hat{D},\hat{C}_n]|\Psi_0^{\mathrm{CC}}\rangle+\langle\overline{\Psi}_0|\hat{C}_n\hat{D}|\Psi_0^{\mathrm{CC}}\rangle,\end{aligned} \tag{78}$$

where $|\Psi_n\rangle=\hat{C}_n|\Psi_0^{\mathrm{CC}}\rangle$ with

$$\hat{C}_n=\sum_I X_{In}\hat{C}_I. \tag{79}$$

As an obvious consequence of the commutator, the first term on the right-hand-side of Eq. (78) is separable. The second term, of course, is not yet separable, but may be rewritten further by using the identity

$$\langle\overline{\Psi}_0|\hat{C}_n\hat{D}|\Psi_0^{\mathrm{CC}}\rangle=\langle\overline{\Psi}_0|\hat{C}_n(\hat{H}-E_0+\omega_n)\times(\hat{H}-E_0+\omega_n)^{-1}\hat{D}|\Psi_0^{\mathrm{CC}}\rangle. \quad (80)$$

Now $(\hat{H}-E_0+\omega_n)^{-1}$ may be replaced by its biorthogonal representation

$$\sum_{I,J}|\Psi_I^0\rangle(\boldsymbol{M}+\omega_n)_{IJ}^{-1}\langle\Psi_J^{\perp}|. \quad (81)$$

Note that the use of the extended representation in terms of $\boldsymbol{M}'$ would make no difference. As a result Eq. (80) becomes

$$\begin{aligned}\langle\overline{\Psi}_0|\hat{C}_n\hat{D}|\Psi_0^{\mathrm{CC}}\rangle&=\sum_{I,J}\langle\overline{\Psi}_0|\hat{C}_n(\hat{H}-E_0+\omega_n)\hat{C}_I|\Psi_0^{\mathrm{CC}}\rangle\\&\quad\times(\boldsymbol{M}+\omega_n)_{IJ}^{-1}\langle\Psi_J^{\perp}|\hat{D}|\Psi_0^{\mathrm{CC}}\rangle\\&=-\sum_{I,J}\langle\overline{\Psi}_0|[[\hat{H},\hat{C}_I],\hat{C}_n]|\Psi_0^{\mathrm{CC}}\rangle\\&\quad\times(\boldsymbol{M}+\omega_n)_{IJ}^{-1}\langle\Psi_J^{\perp}|\hat{D}|\Psi_0^{\mathrm{CC}}\rangle. \quad (82)\end{aligned}$$

To make contact with the original formulation of Koch and Jørgensen Eq. (82) may be written as

$$\langle\overline{\Psi}_0|\hat{C}_n\hat{D}|\Psi_0^{\mathrm{CC}}\rangle=\sum_{I,K}\langle\overline{\Psi}_0|[[\hat{H},\hat{C}_I],\hat{C}_K]|\Psi_0\rangle X_I(-\omega_n)X_{Kn}, \quad (83)$$

where

$$X_I(-\omega_n)=-\sum_J(\boldsymbol{M}+\omega_n)_{IJ}^{-1}\langle\Psi_J^{\perp}|\hat{D}|\Psi_0^{\mathrm{CC}}\rangle. \quad (84)$$

Indeed, as was shown by Koch and Jørgensen, the right transition moment in the form of Eqs. (83) and (84) is size intensive. The compactness property, of course, is not changed by this procedure.

Our findings can be summarized as follows. The bCC representation allows for practical nonperturbative approximation schemes which is a very desirable feature. In comparison with the ADC (ECO-ISR) representation, which, however, has been used only in combination with perturbation theory (for the secular matrix elements and effective transition moments), the CC method has the disadvantages that the secular matrix is non-Hermitian and that the compactness and separability properties are weaker. A relatively complicated formulation of the transition moment is necessary to obtain size-intensive intensities. A consistent third-order description of $\boldsymbol{f}$ requires inclusion of the triple excitations in the explicit configuration space. A consistent third-order CC method referred to as CC3 model that indeed considers the triple excitations though with certain simplifications of the full CC expressions has been developed by Christiansen *et al.*[36]

VI. CONCLUDING REMARKS

The actual potential of the ADC(3) method for treating electronic transitions in larger molecules depends, of course, critically on the inherent computational costs. Clearly, the computational bottleneck is the calculation of the third-order contributions to the p-h block of the secular matrix $\boldsymbol{C}$. As specified by Eqs. (C9)–(C37), there are 29 distinct terms, involving fourfold and partly fivefold summations over orbital indices. The computational cost of this part scales as N^8 with the number N of orbitals (in the rough estimate not distinguishing between occupied and virtual orbitals). A more favorable N^7 scaling is found for generating the p-h/$2p$-$2h$ coupling block. The number of nonvanishing matrix elements of the latter block and of the $2p$-$2h$ block is N^6, so that an iteration step in the diagonalization procedure scales as N^6, that is, as in the familiar SDCI treatment. The much simpler ADC(2) scheme, for example, scales as N^5 in the iteration step and as N^6 in the generation of the p-h block.

The different types of matrix elements in the blocks of $\boldsymbol{C}$ suggest to adopt a mixed strategy for the matrix-times-vector product in the diagonalizer iterations. For the $2p$-$2h$ block, which is linear in the Coulomb integrals, the adequate choice is adopting the integral driven direct diagonalization technique, as used in direct CI methods. The second- and third-order matrix elements in the other blocks should preferably be calculated once and stored on disk. According to an exploratory analysis, their computation can be performed quite efficiently by splitting the summations into subsequent passes through ordered segments of the Coulomb integral list.

A challenge of its own kind is the third-order treatment of the intensities. Though the scaling behavior here, like for the energies, is N^8 and N^7 in the p-h and $2p$-$2h$ parts, respectively, the large number of distinct third-order contributions to $\boldsymbol{f}$ (altogether about 200 terms) causes severe problems even for an error-free implementation in a computer code. While it would be desirable to have consistent third-order transition moments, e.g., for calculating accurate polarizabilities, in normal applications the second-order treatment of the intensities is by far sufficient. This suggests to combine the transition moments of the ADC(2) scheme with the eigenvectors of the ADC(3) secular matrix. Such a scheme will be referred to as ADC(3/2) scheme.

Finally one may wonder about the considerable complexity of the derivation and the final form of the ADC(3) expressions. It seems, however, that what one finds here is reflecting the intrinsic complexity of the excitation problem rather than artificial complications of the method, which, to emphasize it once more, is structurally utmost simple. How reliable are the results presented here? As an effort to cope with this obvious problem, the explicit ADC procedure has been performed independently and individually by each of the authors allowing for threefold mutual checks.

ACKNOWLEDGMENTS

The authors are indebted to V. Bezrukhov who contributed a computer code for generating diagram graphs. This work has been supported by the Deutsche Forschungsgemeinschaft(DFG). One of the authors (A.B.T.) gratefully acknowledges an Alexander von Humboldt fellowship.

$$\begin{pmatrix} 0 & 1 \\ 1 & 0 \end{pmatrix} \quad \begin{pmatrix} 0 & 1 & 0 \\ 1 & 0 & 1 \\ 0 & 1 & 0 \end{pmatrix} \quad \begin{pmatrix} 0 & 0 & 0 & 1 \\ 1 & 0 & 1 & 0 \\ 0 & 2 & 0 & 0 \\ 0 & 0 & 1 & 0 \end{pmatrix} \quad \begin{pmatrix} 0 & 1 & 0 & 0 \\ 0 & 0 & 2 & 0 \\ 0 & 1 & 0 & 1 \\ 1 & 0 & 0 & 0 \end{pmatrix} \quad \begin{pmatrix} 0 & 1 & 0 & 0 \\ 1 & 0 & 1 & 0 \\ 0 & 1 & 0 & 1 \\ 0 & 0 & 1 & 0 \end{pmatrix} \quad \begin{pmatrix} 0 & 1 & 0 & 0 \\ 0 & 0 & 1 & 1 \\ 1 & 1 & 0 & 0 \\ 0 & 0 & 1 & 0 \end{pmatrix} \quad \begin{pmatrix} 0 & 0 & 1 & 0 \\ 1 & 0 & 0 & 1 \\ 0 & 2 & 0 & 0 \\ 0 & 0 & 1 & 0 \end{pmatrix}$$

(0) (1) A B C D E

FIG. 7. Matrix representation (adjacency matrices) of the zeroth-, first-, and second-order Feynman diagrams for the polarization propagator.

APPENDIX A: DIAGRAMMATIC RULES

The rules for drawing and evaluating Feynman diagrams (FD) are well documented in textbooks (for example, see Fetter and Walecka[1]). The rules for the associated time-ordered or Goldstone diagrams (GD) are less familiar (for the GD rules in the case of the electron propagator see Cederbaum[45]). For the case of the polarization propagator the Feynman and Goldstone diagram rules have been amply described in Appendix A of Ref. 11, and for brevity we may refer the reader to this source. However, here the following corrections concerning the overall sign of a diagram must be made:

The rule (F4) should read:

(F4) Multiply by a sign factor $(-1)^L$, where L is the number of closed (Fermion) loops, and by an additional factor $(-i)$ stemming from the definition of the polarization propagator. When all i factors for the nth order diagram are collected one obtains the overall factor

$$(-i)(-i)^n(+i)^{2n+1}=i^{n+1}.$$

An additional factor (-1) applies if one Fermion line runs from the bottom (lower external vertex) to the top (upper external vertex) of the diagram (in this case another Fermion line runs from the top to the bottom; this is opposed to the case where the Fermion lines run from top to top and from bottom to bottom.)

In a similar way the GD rule (G4) has to be modified:

(G4) Each hole line introduces the factor (-1). Thus, multiply by a sign factor $(-1)^{L+M}$, where L is the number of closed loops and M is the number of hole lines. Since each (inner) vertex gives a factor $(-i)$ and each cut gives a factor $(+i)$, one obtains together with the factor $(-i)$ from the definition (of the polarization propagator) the overall factor simply as

$$(-i)(-i)^n(+i)^{n+1}=+1.$$

An additional factor (-1) applies if one (or two) Fermion line(s) run between the two external vertices.

For illustration we consider the time ordering $(10a)$ of the RPA diagram (7) (Fig. 4). The analytical expression reads

$$D^{7.10a}_{ak,mb} \equiv (-1)(\omega-\epsilon_a-\epsilon_k)^{-1}(\epsilon_m+\epsilon_k-\epsilon_a-\epsilon_b)^{-1} \times \sum_{\substack{ij \\ cd}} V_{ai[ck]}V_{cj[di]}V_{db[mj]}(\epsilon_m+\epsilon_i-\epsilon_b-\epsilon_c)^{-1} \times (\epsilon_m+\epsilon_j-\epsilon_b-\epsilon_d)^{-1}.$$

Obviously this term is of the form (A_2) (Table II) and one may readily extract the corresponding contribution to $f^{(3)}_{ak,mb}$.

APPENDIX B: COMPUTER GENERATION OF DIAGRAMS

The matrix representation of Feynman diagrams (FD) in Abrikosov (or Hugenholtz) notation presented in the following is based on the concept of adjacency matrices of graph theory (see, for example, Harary[46]). The use of adjacency matrices in the computer generation of Feynman diagrams has been discussed by Paldus and Wong.[47,48] Using a somewhat different method than the one described below the latter authors have generated a complete list of third-order diagrams for the polarization propagator.[48]

According to the following prescription one may map a given nth order FD uniquely to a quadratic $(n+2)$ matrix:

(i) Label the $n+2$ vertices of the FD by the numbers $1,2,\ldots,n+2$, beginning with the top (outer) vertex and ending with the bottom (outer) vertex.

(ii) Form a quadratic $(n+2)$ matrix $\boldsymbol{S}$ where S_{ij} is the number of $G^{(0)}$ lines running from vertex i to vertex j. All other entries are set to zero.

(iii) Optionally an extra symbol can be used as an entry in $S_{1,n+2}$ to indicate the auxiliary ω-line connecting the two outer vertices.

Figure 7 shows the adjacency matrices for the FDs through second order.

The following properties can readily be verified:

(1) The matrix elements S_{ij} can assume only the values 0, 1, or 2; Diagonal elements vanish: $S_{ii}=0$. For inner vertices $i,j=2,\ldots,n+1$, the row sum and the column sum is 2. For the (outer) vertices 1 and $n+2$ the row and column sum is 1.

(2) Different diagrams are mapped to different matrices, that is, the mapping is one-to-one for the range of images.

(3) A matrix fulfilling the properties (1) does not necessarily correspond to a FD. For example, the corresponding diagram may be unlinked; different matrices may belong to the same FD.

(4) Time orderings of a FD correspond to simultaneous permutations of rows and columns in the original matrix.

Based on these properties one can readily devise an algorithm for generating all FDs of a given order. One simply constructs all matrices with the properties (1) and then discards any matrix not qualifying for a FD or being only a different time ordering of a previous FD. For each nth order FD one obtains a matrix representation of the $(n+2)!$ Goldstone diagrams by performing all simultaneous row and column permutations of the original matrix. Finally each matrix can be converted into a symbolic form specifying the Coulomb integral products and the ω-denominators of the corresponding analytical expressions. This allows one to sort the

diagrams into groups of the same integral product type. A complete specification of the final analytic expression including the overall sign has not been attempted.

APPENDIX C: ADC(3) EXPRESSIONS FOR $K+C$

In the following we collect the expressions for the secular matrix $\boldsymbol{K}+\boldsymbol{C}$ (effective interaction) of the third-order ADC scheme for $\boldsymbol{\Pi}^{+}$. (A complete list for both $\boldsymbol{K}+\boldsymbol{C}$ and $\boldsymbol{f}$ is available at our website.[38]) The explicit ADC(3) configuration space comprises the $1h$ and $2h$-$1p$ configurations. For notational brevity we use the short-hand notation

$$v_{pqrs}=\frac{V_{pq[rs]}}{\epsilon_p+\epsilon_q-\epsilon_r-\epsilon_s}, \tag{C1}$$

where $V_{pq[rs]}=V_{pqrs}-V_{pqsr}$ and ϵ_p denote the antisymmetrized Coulomb integrals in ''1212'' notation and HF orbital energies, respectively. The letters $i,j,k,l,\ldots$ and $a,b,c,\ldots$ refer to occupied and unoccupied orbitals, respectively. The subscripts $p,q,r,\ldots$ label both occupied and unoccupied orbitals.

p-h block:

zeroth through second order (see Ref. 11)

$$K_{ak,a'k'}=(\epsilon_a-\epsilon_k)\,\delta_{aa'}\delta_{kk'}, \tag{C2}$$

$$C^{(1)}_{ak,a'k'}=-V_{ak'[a'k]}, \tag{C3}$$

$$C^{(2)}_{ak,a'k'}=C^{(A)}_{ak,a'k'}+C^{(B)}_{ak,a'k'}+C^{(C)}_{ak,a'k'}, \tag{C4}$$

where

$$C^{(A)}_{ak,a'k'}=\frac{1}{2}\,\delta_{kk'}\sum_{\substack{c\\ i,j}} v_{acij}v_{ija'c}\left(\epsilon_i+\epsilon_j-\epsilon_c-\frac{1}{2}(\epsilon_a+\epsilon_{a'})\right), \tag{C5}$$

$$C^{(B)}_{ak,a'k'}=\frac{1}{2}\,\delta_{aa'}\sum_{\substack{c,d\\ i}} v_{cdki}v_{k'icd}\left(\frac{1}{2}(\epsilon_k+\epsilon_{k'})+\epsilon_i-\epsilon_c-\epsilon_d\right), \tag{C6}$$

$$C^{(C)}_{ak,a'k'}=\sum_{c,i} v_{k'ia'c}v_{acik}\left(\frac{1}{2}(\epsilon_k+\epsilon_{k'}-\epsilon_a-\epsilon_{a'})+\epsilon_i-\epsilon_c\right). \tag{C7}$$

Third-order:

there are 29 contributions

$$C^{(3)}_{ak,a'k'}=\sum_{i=1}^{29} C^{(3,i)}_{ak,a'k'}, \tag{C8}$$

as specified below [Eqs. (C9)–(C37)]. Note that the expressions given here correspond to a Hermitian $\boldsymbol{f_{11}}$ block [see Eq. (26)]. The terms are ordered according to their diagrammatic origin.

diagrams (1)–(6)

$$C^{(3,1)}_{ak,a'k'}=\frac{1}{4}\,\delta_{aa'}\sum_{\substack{c,d\\ i,j,m}} v_{ijcd}V_{k'm[ij]}v_{cdkm}\times\left(\frac{\epsilon_m-\epsilon_c-\epsilon_d+(1/2)(\epsilon_k+\epsilon_{k'})}{\epsilon_{k'}+\epsilon_m-\epsilon_c-\epsilon_d}\right)+\text{h.c.}, \tag{C9}$$

$$C^{(3,2)}_{ak,a'k'}=\frac{1}{8}\,\delta_{aa'}\sum_{\substack{c,d,f,g\\ i}} V_{cd[fg]}\times\left(\frac{v_{fgki}V_{k'i[cd]}}{\epsilon_k+\epsilon_i-\epsilon_c-\epsilon_d}+\frac{v_{k'icd}V_{fg[ik]}}{\epsilon_{k'}+\epsilon_i-\epsilon_g-\epsilon_f}\right), \tag{C10}$$

$$C^{(3,3)}_{ak,a'k'}=\delta_{aa'}\sum_{\substack{c,d,f\\ i,j}} v_{cdij}v_{k'jcf}V_{if[dk]}\times\left(\frac{\epsilon_j-\epsilon_c-\epsilon_f+(1/2)(\epsilon_k+\epsilon_{k'})}{\epsilon_k+\epsilon_j-\epsilon_c-\epsilon_f}\right)+\text{h.c.}, \tag{C11}$$

$$C^{(3,4)}_{ak,a'k'}=\frac{1}{2}\,\delta_{aa'}\sum_{\substack{c,d,f\\ i,j}} V_{cj[fi]}\times\left(\frac{v_{dfkj}V_{k'i[cd]}}{\epsilon_k+\epsilon_i-\epsilon_c-\epsilon_d}+\frac{v_{k'icd}V_{fd[kj]}}{\epsilon_{k'}+\epsilon_j-\epsilon_d-\epsilon_f}\right), \tag{C12}$$

$$C^{(3,5)}_{ak,a'k'}=\frac{1}{4}\,\delta_{kk'}\sum_{\substack{c,d,f\\ i,j}} v_{cdij}v_{ija'f}V_{af[cd]}\times\left(\frac{\epsilon_i+\epsilon_j-\epsilon_f-(1/2)(\epsilon_a+\epsilon_{a'})}{\epsilon_i+\epsilon_j-\epsilon_a-\epsilon_f}\right)+\text{h.c.}, \tag{C13}$$

$$C^{(3,6)}_{ak,a'k'}=\frac{1}{8}\,\delta_{kk'}\sum_{\substack{c\\ i,j,m,l}} V_{lm[ij]}\times\left(\frac{v_{acln}V_{ij[a'c]}}{\epsilon_i+\epsilon_j-\epsilon_a-\epsilon_c}-\frac{v_{ija'c}V_{ac[lm]}}{\epsilon_m+\epsilon_l-\epsilon_{a'}-\epsilon_c}\right), \tag{C14}$$

$$C^{(3,7)}_{ak,a'k'}=\delta_{kk'}\sum_{\substack{c,d\\ i,j,m}} v_{cdij}v_{ima'd}V_{aj[mc]}\times\left(\frac{\epsilon_i+\epsilon_m-\epsilon_d-(1/2)(\epsilon_a+\epsilon_{a'})}{\epsilon_i+\epsilon_m-\epsilon_a-\epsilon_d}\right)+\text{h.c.}, \tag{C15}$$

$$C^{(3,8)}_{ak,a'k'}=\frac{1}{2}\,\delta_{kk'}\sum_{\substack{c,d\\ i,j,m}} V_{mc[id]}\times\left(\frac{v_{adjm}V_{ij[a'c]}}{\epsilon_i+\epsilon_j-\epsilon_a-\epsilon_c}+\frac{v_{ija'c}V_{ad[mj]}}{\epsilon_j+\epsilon_m-\epsilon_{a'}-\epsilon_d}\right), \tag{C16}$$

$$C^{(3,9)}_{ak,a'k'}=\frac{1}{2}\sum_{\substack{c,d\\ i,j,m}} v_{ijcd}v_{cdjm}(\delta_{aa'}V_{k'm[ki]}-\delta_{kk'}V_{am[a'i]}), \tag{C17}$$

$$C^{(3,10)}_{ak,a'k'}=\frac{1}{2}\sum_{\substack{c,d,f\\ i,j}} v_{ijcd}v_{dfij}(\delta_{aa'}V_{ck'[kf]}+\delta_{kk'}V_{ac[a'f]}), \tag{C18}$$

$$C^{(3,11)}_{ak,a'k'}=\frac{1}{2}\sum_{\substack{c,d,f\\ i,j}} v_{ijcd}V_{cd[fj]}\frac{1}{\epsilon_i-\epsilon_f}\times(\delta_{aa'}V_{k'f[ik]}+\delta_{kk'}V_{af[a'i]})+\text{h.c.}, \tag{C19}$$

$$C^{(3,12)}_{ak,a'k'} = \frac{1}{2}\sum_{\substack{c,d\\ i,j,m}} v_{ijcd} V_{md[ij]} \frac{1}{\epsilon_m - \epsilon_c} \times (\delta_{aa'} V_{k'c[km]} - \delta_{kk'} V_{ac[a'm]}) + \text{h.c.}, \tag{C20}$$

diagram (7)

$$C^{(3,13)}_{ak,a'k'} = \frac{1}{2}\sum_{\substack{c,d\\ i,j}} v_{cdij} V_{aj[ck]} V_{ik'[a'd]} \frac{1}{\epsilon_k + \epsilon_i - \epsilon_a - \epsilon_d} + \text{h.c.}, \tag{C21}$$

$$C^{(3,14)}_{ak,a'k'} = \frac{1}{2}\sum_{\substack{c,d\\ i,j}} V_{jc[id]} \times \left(\frac{v_{adjk} V_{ik'[a'c]}}{\epsilon_k + \epsilon_i - \epsilon_a - \epsilon_c} + \frac{v_{ik'ca'} V_{ad[jk]}}{\epsilon_{k'} + \epsilon_j - \epsilon_{a'} - \epsilon_d} \right), \tag{C22}$$

diagrams (8) and (9)

$$C^{(3,15)}_{ak,a'k'} = \frac{1}{4}\sum_{\substack{c,d\\ i,j}} v_{acij} v_{ijcd} V_{dk'[a'k]} + \text{h.c.}, \tag{C23}$$

$$C^{(3,16)}_{ak,a'k'} = \frac{1}{2}\sum_{\substack{c,d\\ i,j}} v_{cdij} V_{ja[cd]} V_{ik'[a'k]} \frac{1}{\epsilon_i - \epsilon_a} + \text{h.c.}, \tag{C24}$$

$$C^{(3,17)}_{ak,a'k'} = \frac{1}{2}\sum_{\substack{c\\ i,j,m}} v_{acjm} V_{jm[ic]} V_{ik'[a'k]} \frac{1}{\epsilon_i - \epsilon_a} + \text{h.c.}, \tag{C25}$$

diagrams (10) and (11)

$$C^{(3,18)}_{ak,a'k'} = \frac{1}{4}\sum_{\substack{c,d\\ i,j}} v_{cdjk} v_{ijcd} V_{ak'[a'i]} + \text{h.c.}, \tag{C26}$$

$$C^{(3,19)}_{ak,a'k'} = \frac{1}{2}\sum_{\substack{c,d\\ i,j}} v_{cdij} V_{ij[dk]} V_{k'a[ca']} \frac{1}{\epsilon_k - \epsilon_c} + \text{h.c.}, \tag{C27}$$

$$C^{(3,20)}_{ak,a'k'} = \frac{1}{2}\sum_{\substack{c,d,f\\ i}} v_{dfik} V_{ci[df]} V_{ak'[ca']} \frac{1}{\epsilon_k - \epsilon_c} + \text{h.c.}, \tag{C28}$$

diagrams (12) and (13)

$$C^{(3,21)}_{ak,a'k'} = \sum_{\substack{c,d\\ i,j}} v_{adij} v_{ik'a'c} V_{cj[dk]} \times \left(\frac{\epsilon_i - \epsilon_c + (1/2)(\epsilon_k + \epsilon_{k'} - \epsilon_a - \epsilon_{a'})}{\epsilon_k + \epsilon_i - \epsilon_a - \epsilon_c} \right) + \text{h.c.}, \tag{C29}$$

$$C^{(3,22)}_{ak,a'k'} = \sum_{\substack{c,d\\ i,j}} v_{cdjk} v_{ik'a'c} V_{ja[di]} \times \left(\frac{\epsilon_i - \epsilon_c + (1/2)(\epsilon_k + \epsilon_{k'} - \epsilon_a - \epsilon_{a'})}{\epsilon_k + \epsilon_i - \epsilon_a - \epsilon_c} \right) + \text{h.c.}, \tag{C30}$$

diagrams (14) and (15)

$$C^{(3,23)}_{ak,a'k'} = \frac{1}{2}\sum_{\substack{c,d,f\\ i}} v_{cdik} v_{k'ia'f} V_{af[cd]} \times \left(\frac{\epsilon_i - \epsilon_f + (1/2)(\epsilon_k + \epsilon_{k'} - \epsilon_a - \epsilon_{a'})}{\epsilon_k + \epsilon_i - \epsilon_a - \epsilon_f} \right) + \text{h.c.}, \tag{C31}$$

$$C^{(3,24)}_{ak,a'k'} = \frac{1}{2}\sum_{\substack{c\\ i,j,m}} v_{acij} v_{k'mca'} V_{ij[km]} \times \left(\frac{\epsilon_m - \epsilon_c + (1/2)(\epsilon_k + \epsilon_{k'} - \epsilon_a - \epsilon_{a'})}{\epsilon_k + \epsilon_m - \epsilon_a - \epsilon_c} \right) + \text{h.c.}, \tag{C32}$$

diagram (16)

$$C^{(3,25)}_{ak,a'k'} = \tfrac{1}{2}\sum_{\substack{c,d\\ i,j}} v_{acij} v_{ijda'} V_{dk'[ck]}, \tag{C33}$$

diagram (17)

$$C^{(3,26)}_{ak,a'k'} = \tfrac{1}{2}\sum_{\substack{c,d\\ i,j}} v_{cdik} v_{k'jcd} V_{ai[a'j]}, \tag{C34}$$

diagram (18)

$$C^{(3,27)}_{ak,a'k'} = \sum_{\substack{c\\ i,j,m}} v_{acij} v_{jma'c} V_{ik'[km]}, \tag{C35}$$

diagram (19)

$$C^{(3,28)}_{ak,a'k'} = \sum_{\substack{c,d,f\\ i}} v_{cdki} v_{ik'df} V_{af[a'c]}, \tag{C36}$$

diagrams (22) and (23)

$$C^{(3,29)}_{ak,a'k'} = \sum_{\substack{c,d\\ i,j}} v_{acij} v_{jk'cd} V_{di[a'k]} + \text{h.c.}. \tag{C37}$$

The contributions (C9)–(C20) are related to the ADC quantities of the one-particle Green's function according to Eq. (35). In particular, one may note the relation

$$\sum_{\mu=9}^{12} C^{(3,\mu)}_{ak,a'k'} = -\delta_{aa'}\Sigma^{(3)}_{k'k}(\infty) + \delta_{kk'}\Sigma^{(3)}_{aa'}(\infty),$$

where $\Sigma^{(3)}_{pq'}(\infty)$ is the so-called static self-energy (see Ref. 39).

$1p$-$1h$/$2p$-$2h$ coupling block:

$$C^{(1)}_{ak,a'b'k'l'} = \delta_{aa'} V_{k'l'[kb']} - \delta_{ab'} V_{k'l'[ka']} - \delta_{kk'} V_{al'[a'b']} + \delta_{kl'} V_{ak'[a'b']}, \tag{C38}$$

$$C^{(2)}_{ak,a'b'k'l'} = \sum_{i=1}^{5} C^{(2,i)}_{ak,a'b'k'l'}, \tag{C39}$$

where

$$C^{(2,1)}_{ak,a'b'k'l'} = \left(\left(\delta_{aa'} \sum_{c,i} v_{k'ib'c} V_{l'c[ik]} \right) - (a' \leftrightarrow b') \right) - (k' \leftrightarrow l'), \tag{C40}$$

$$C^{(2,2)}_{ak,a'b'k'l'} = \left(\frac{1}{2} \delta_{aa'} \sum_{c,d} v_{k'l'cd} V_{cd[kb']} \right) - (a' \leftrightarrow b'), \tag{C41}$$

$$C^{(2,3)}_{ak,a'b'k'l'} = \left(\left(\delta_{kk'} \sum_{c,i} v_{l'ib'c} V_{ac[ia']} \right) - (a' \leftrightarrow b') \right) - (k' \leftrightarrow l'), \tag{C42}$$

$$C^{(2,4)}_{ak,a'b'k'l'} = \left(\frac{1}{2} \delta_{kk'} \sum_{i,j} v_{ija'b'} V_{l'a[ij]} \right) - (k' \leftrightarrow l'), \tag{C43}$$

$$C^{(2,5)}_{ak,a'b'k'l'} = \left(\sum_{c} v_{k'l'a'c} V_{ac[b'k]} \right) - (a' \leftrightarrow b'), \tag{C44}$$

$$C^{(2,6)}_{ak,a'b'k'l'} = \left(\sum_{i} v_{l'ia'b'} V_{ak'[ik]} \right) - (k' \leftrightarrow l'). \tag{C45}$$

Here $(p \leftrightarrow q)$ means repeating the preceding term, but with p and q interchanged. $2p$-$2h$ block:

$$\begin{aligned} K_{abkl,a'b'k'l'} &= (\epsilon_a + \epsilon_b - \epsilon_k - \epsilon_l) \delta_{aa'} \delta_{bb'} \delta_{kk'} \delta_{ll'} \\ C^{(1)}_{abkl,a'b'k'l'} &= \delta_{kk'} \delta_{ll'} V_{ab[a'b']} + \delta_{aa'} \delta_{bb'} V_{k'l'[kl]} \\ &\quad - (\delta_{bb'} \delta_{ll'} V_{ak'[a'k]} + \delta_{bb'} \delta_{kk'} V_{al'[a'l]} \\ &\quad + \delta_{aa'} \delta_{ll'} V_{bk'[b'k]} + \delta_{aa'} \delta_{kk'} V_{bl'[b'l]}) \\ &\quad + (k' \leftrightarrow l') + (a' \leftrightarrow b') - (k' \leftrightarrow l', a' \leftrightarrow b'). \end{aligned} \tag{C46}$$

It should be noted that the relative signs have been chosen in such a way that the first-order contributions to $\boldsymbol{C}$ agree with

$$C^{(1)}_{IJ} = \langle \Phi_I | \hat{H} - E_0(1) | \Phi_J \rangle,$$

where $\{|\Phi_J\rangle\} \equiv \{c_a^\dagger c_k |\Phi_0^N\rangle, c_a^\dagger c_b^\dagger c_k c_l |\Phi_0^N\rangle, \ldots\}$ are the usual N-electron HF configurations and $E_0(1)$ is the first-order ground-state energy.

[1] A. L. Fetter and J. D. Walecka, *Quantum Theory of Many-Particle Systems* (McGraw Hill, New York, 1971).
[2] P. Jørgensen and J. Simons, *Second Quantization-Based Methods in Quantum Chemistry* (Academic, New York, 1981).
[3] R. McWeeny, *Methods of Molecular Quantum Mechanics* (Academic, London, 1989).
[4] D. J. Rowe, Rev. Mod. Phys. **40**, 153 (1968).
[5] J. Rose, T. Shibuya, and V. McKoy, J. Chem. Phys. **58**, 74 (1973).
[6] C. W. McCurdy, T. N. Rescigno, D. L. Yeager, and V. McKoy, in *Methods of Electronic Structure Theory*, edited by H. F. Schaefer (Plenum, New York, 1977).
[7] M. F. Herman, K. F. Freed, and D. L. Yeager, Adv. Chem. Phys. **48**, 1 (1981).
[8] D. Goscinski and B. Lukman, Chem. Phys. Lett. **7**, 573 (1970).
[9] J. Oddershede, Adv. Quantum Chem. **11**, 275 (1978).
[10] J. Oddershede, P. Jørgensen, and D. L. Yeager, Comput. Phys. Rep. **2**, 33 (1984).
[11] J. Schirmer, Phys. Rev. A **26**, 2395 (1982).
[12] E. S. Nielsen, P. Jørgensen, and J. Oddershede, J. Chem. Phys. **73**, 6238 (1980).
[13] J. Oddershede, Adv. Phys. Chem. **69**, 201 (1987).
[14] A. B. Trofimov and J. Schirmer, J. Phys. B **28**, 2299 (1995).
[15] J. Oddershede and P. Jørgensen, J. Chem. Phys. **66**, 1541 (1977).
[16] K. Andersson, P.-Å Malmquist, B. O. Roos, A. Sadlej, and K. Wolinski, J. Phys. Chem. **94**, 5483 (1990).
[17] K. Andersson, P.-Å Malmquist, and B. O. Roos, J. Chem. Phys. **96**, 1218 (1992).
[18] L. S. Cederbaum and W. Domcke, Adv. Chem. Phys. **36**, 205 (1977).
[19] Y. Öhrn and G. Born, Adv. Quantum Chem. **13**, 1 (1981).
[20] W. von Niessen, J. Schirmer, and L. S. Cederbaum, Comput. Phys. Rep. **1**, 59 (1984).
[21] J. Simons, Annu. Rev. Phys. Chem. **28**, 1 (1977).
[22] F. Mertins and J. Schirmer, Phys. Rev. A **53**, 2140 (1996).
[23] D. Mukherjee and P. K. Mukherjee, Chem. Phys. **39**, 325 (1979).
[24] S. Gosh, D. Mukherjee, and D. Bhattacheryya, Chem. Phys. **72**, 161 (1982).
[25] H. Nakatsuji and K. Hirao, Chem. Phys. Lett. **47**, 569 (1977).
[26] H. Nakatsuji, Chem. Phys. Lett. **67**, 329 (1979).
[27] H. Nakatsuji, Chem. Phys. Lett. **67**, 334 (1984).
[28] E. Dalgaard and H. J. Monkhorst, Phys. Rev. A **28**, 1217 (1983).
[29] H. Koch and P. Jørgensen, J. Chem. Phys. **93**, 3333 (1990).
[30] H. Koch, H. J. A. Jensen, P. Jørgensen, and T. Helgaker, J. Chem. Phys. **93**, 3345 (1990).
[31] H. J. Monkhorst, Int. J. Quantum Chem., Symp. **11**, 421 (1977).
[32] A. E. Kondo, P. Piecuch, and J. Paldus, J. Chem. Phys. **102**, 6511 (1995).
[33] H. Sekino and R. J. Bartlett, Int. J. Quantum Chem., Symp. **18**, 255 (1984).
[34] J. Geertsen, M. Rittby, and R. J. Bartlett, Chem. Phys. Lett. **164**, 57 (1989).
[35] J. F. Stanton and R. J. Bartlett, J. Chem. Phys. **98**, 7029 (1993).
[36] O. Christiansen, H. Koch, and P. Jørgensen, J. Chem. Phys. **103**, 7429 (1995).
[37] Program written by V. Bezrukhov.
[38] www.pci.uni-heidelberg.de/tc/html/adc3pp.html
[39] J. Schirmer, A. B. Trofimov, and G. Stelter, J. Chem. Phys. **109**, 4734 (1998).
[40] J. Schirmer and F. Mertins, J. Phys. B **29**, 3559 (1996).
[41] J. Schirmer, Phys. Rev. A **43**, 4647 (1991).
[42] J. Schirmer and F. Mertins, Int. J. Quantum Chem. **58**, 329 (1996).
[43] F. Mertins, J. Schirmer, and A. Tarantelli, Phys. Rev. A **53**, 2153 (1996).
[44] H. Koch, R. Kobayashi, A. Sanchez de Merás, and P. Jørgensen, J. Chem. Phys. **100**, 4393 (1994).
[45] L. S. Cederbaum, Theor. Chim. Acta **31**, 229 (1973).
[46] F. Harary, *Graph Theory* (Addison-Wesley, Reading, Mass. 1969).
[47] J. Paldus and H. C. Wong, Comput. Phys. Commun. **6**, 1 (1973).
[48] H. C. Wong and J. Paldus, Comput. Phys. Commun. **6**, 9 (1973).